

SPECIAL TOPIC: Trans-scale RNA regulation and imaging

RESEARCH PAPER

TurboID-based proximity labeling identifies novel germline proteins that maintain E granule integrity and small RNA homeostasis in *C. elegans*



Kun Li^{1†}, Xuezhu Feng^{2†}, Ke Wang^{3†}, Xiaona Huang¹, Liang Liu¹, Chaoyue Yan¹, Xinya Huang¹, Chengming Zhu^{4*}, Quan Wen^{1*}, Shouhong Guang^{1*} & Xiangyang Chen^{1*}

¹Department of Obstetrics and Gynecology, The First Affiliated Hospital of USTC, The USTC RNA Institute, Ministry of Education Key Laboratory for Membraneless Organelles & Cellular Dynamics, Hefei National Research Center for Physical Sciences at the Microscale, Center for Advanced Interdisciplinary Science and Biomedicine of IHM, School of Life Sciences, Division of Life Sciences and Medicine, University of Science and Technology of China. Hefei 230027. China

†Contributed equally to this work

*Corresponding authors (Chengming Zhu, email: zcm916@ustc.edu.cn; Quan Wen, email: qwen@ustc.edu.cn; Shouhong Guang, email: sguang@ustc.edu.cn; Xiangyang Chen, email: xychen91@ustc.edu.cn)

Received 25 April 2025; Accepted 9 July 2025; Published online 10 October 2025

Germ granules are biomolecular condensates composed of RNA and proteins that play crucial roles in RNA metabolism and post-transcriptional gene regulation. *C. elegans* germ granules consist of multiple distinct subcompartments, including P granules, *Mutator* foci, Z granules, SIMR foci, P-bodies, D granules, and E granules. Among these condensates, the E granule, which is nonrandomly positioned within the germ granule, is required for the production of a specialized class of small interfering RNAs (siRNAs). However, the mechanisms underlying E granule formation and its functional significance remain largely unexplored. In this study, via the use of TurboID-based proximity labeling technology combined with an RNAi-based reverse genetic screen, we identified two novel components of the E granule, EGC-2/C27B7.5 and EGC-3/F59G1.8, which initiate E granule assembly. The depletion of EGC-2 or EGC-3 disrupts the perinuclear localization of the EGO and PICS complexes, both of which are enriched in E granules and are required for E-class siRNA and piRNA biogenesis, respectively. Small RNAomic analyses revealed that both EGC-2 and EGC-3 promote the production of 5′ E-class siRNA, whereas piRNA accumulation is inhibited by EGC-3. Taken together, our results elucidate the roles of EGC-2 and EGC-3 in maintaining E granule integrity and small RNA homeostasis. Additionally, the combination of proximity labeling technology and reverse genetic screening provides a robust strategy for studying the assembly of biomolecular condensates.

biomolecular condensates | phase separation | proximity labeling | germ granule | E granule | turboID | siRNA | piRNA.

INTRODUCTION

Biomolecular condensates are micron-scale membraneless organelles (MLOs) present in eukaryotic cells, common examples of which include processing bodies, stress granules, nucleoli, Cajal bodies, and germ granules (Banani et al., 2017; Boeynaems et al., 2018; Ruan et al., 2024; Shin and Brangwynne, 2017). Current models posit that the formation of the biomolecular condensate is driven by liquid-liquid phase separation (LLPS) via multivalent interactions between RNAs, intrinsically disordered proteins, and RNA-binding proteins (Banani et al., 2017; Toretsky and Wright, 2014). These biomolecular condensates help cells spatiotemporally compartmentalize proteins and RNA molecules within distinct subcellular compartments to coordinate complicated

RNA metabolism and gene expression processes (Banani et al., 2017; Dodson and Kennedy, 2020; Standart and Weil, 2018; Zhang and Wang, 2023). Furthermore, many biomolecular condensates contain distinct immiscible subcompartments, forming multilayered architectures, which may regulate sequential RNA processing events; for example, distinct subdomains of the nucleolus participate in different ribosomal RNA processing steps (Fare et al., 2021; Lafontaine et al., 2021; Yanagawa and Shimobayashi, 2024). However, the molecular mechanisms underlying the formation of these multilayered condensates and their cellular functions are still largely unknown.

Germ granules are RNA-rich biomolecular condensates that are anchored on the periphery of the nucleus and are thought to act as organizational hubs for posttranscriptional gene regula-

Citation: Li, K., Feng, X., Wang, K., Huang, X., Liu, L., Yan, C., Huang, X., Zhu, C., Wen, Q., Guang, S., et al. TurboID-based proximity labeling identifies novel germline proteins that maintain E granule integrity and small RNA homeostasis in *C. elegans*. Sci China Life Sci, https://doi.org/10.1007/s11427-025-3025-6



²School of Basic Medical Sciences, Anhui Medical University, Hefei 230032, China

³School of Life Science and Engineering, Jining University, Qufu 273155, China

⁴School of Life Sciences, Anhui Medical University, Hefei 230032, China

tion (Eddy, 1974; Eddy, 1975; Phillips et al., 2022; Voronina et al., 2011). Germ granules are widely present in many animals, including worms, flies, zebrafish, Xenopus and mice (Dodson and Kennedy, 2020; Kemph and Lynch, 2022; Lehmann, 2016; Mukherjee and Mukherjee, 2021; Phillips et al., 2022). In C. elegans, recent studies have shown that germ granules are divided into multiple subcompartments, including P granules, Z granules, Mutator foci, SIMR foci, D granules, E granules, and Pbodies. The P granule is the first membraneless organelle found to be formed by liquid-liquid phase separation and to exhibit liquidlike behaviors, including fusion, dripping, and wetting (Brangwynne et al., 2009). P granules are thought to be major sites of mRNA regulation in germ cells and serve as hubs for self-/nonself RNA discrimination via siRNAs and the RNA interference (RNAi) machinery on the bases of multiple Agonautes (Liu et al., 2023; Phillips et al., 2022; Seroussi et al., 2023; Sundby et al., 2021). PGL-1 is a germline-expressed protein that is a P granule component at all stages of development and is widely used as a marker protein of P granules (Aoki et al., 2021; Kawasaki et al., 1998; Wan et al., 2018). Z granules, marked by the conserved SF1 helicase ZNFX-1, are reported to be adjacent to P granules, and regulate RNAi inheritance (Marnik et al., 2022; Wan et al., 2018). Mutator foci (marked by MUT-16) and E granules (marked by ELLI-1) are two independent germ granule subcompartments that promote the production of siRNAs targeting distinct subsets of germline RNAs, respectively (Chen et al., 2024; Phillips et al., 2012; Uebel et al., 2018; Zhang et al., 2011). SIMR foci, marked by SIMR-1, act downstream of the piRNA pathway to promote siRNA amplification via the Mutator complex and drive small RNA specificity for nuclear Argonaute proteins (Chen and Phillips, 2024; Chen and Phillips, 2025; Manage et al., 2020). P-bodies, which are marked by CGH-1 and are found to be located on top of P granules in pachytene cells, regulate translation and promote small RNA-based transgenerational gene silencing (Du et al., 2023; Gajjar et al., 2025). D granules, marked by DDX-19, are reported to concentrate between the zones of P granules and the nuclear pore complexes (NPCs), forming a tripartite architecture (Huang et al., 2025; Lu et al., 2025; Sheth et al., 2010). Intriguingly, these immiscible germ granule subcompartments are not randomly ordered with respect to each other. For instance, many germ granules contain a single Z granule sandwiched between a P granule and a Mutator focus, forming ordered tri-condensate assemblages termed PZM (Wan et al., 2018). SIMR foci are also found to be spatially organized, adjacent to Z granules and Mutator foci, and opposite P granules (Manage et al., 2020). Moreover, a recent study discovered a toroidal P granule morphology in the midand late pachytene regions of the germline, which encircles the other germ granule compartments in a consistent exterior-tointerior spatial organization, further revealing the hierarchical organization of germ granules (Uebel et al., 2023). Nucleoporins are reported to promote the perinuclear anchoring of germ granules in C. elegans (Lu et al., 2025; Shi et al., 2025; Thomas et al., 2025; Updike and Strome, 2009; Voronina and Seydoux, 2010). Additionally, LOTUS domain proteins, including MIP-1, MIP-2, and LOTR-1, are also required for the perinuclear assembly of particular germ granule compartments (Cipriani et al., 2021; Huang et al., 2025; Marnik et al., 2022; Price et al., 2021). Animals lacking MIP-1 and MIP-2 exhibit temperaturesensitive embryonic lethality, sterility, and mortal germlines, suggesting that the perinuclear anchoring of germ granules is

essential for germ cell development (Cipriani et al., 2021; Price et al., 2021). Interestingly, a recent study reported that a novel germline protein, HERD-1, regulates multiphase condensate immiscibility to mediate small RNA-driven transgenerational epigenetic inheritance, suggesting that the multiphasic architecture of the germ granule is crucial for gene expression regulation (Zhao et al., 2024). The current model posits that the multiphasic architecture of *C. elegans* germ granules helps cells organize numerous perinuclear proteins and coordinate highly sophisticated perinuclear gene regulation networks, especially small RNA-based gene regulatory pathways (Ouyang et al., 2022; Phillips et al., 2022; Sundby et al., 2021).

Although the molecular mechanisms of the assembly of biomolecular condensates have been widely investigated, the cellular functions of many biomolecular condensates and the biological significance of the positioning of proteins in these condensates are still largely unknown. Deciphering the genetic requirements of the assembly of particular condensates may help elucidate the biological functions of these membraneless organelles. For example, RNA-binding proteins such as GLH-1, PGL-1/PGL-3, and MEG-3/MEG-4, play important roles in the formation of P granules (Chen et al., 2020; Folkmann et al., 2021; Hanazawa et al., 2011; Updike and Strome, 2010; Updike and Strome, 2009; Wang et al., 2014). The depletion of these assembly factors usually leads to disordered expression of RNAomes, including small RNAs and mRNAs (Chen et al., 2022; Dai et al., 2022; Dodson and Kennedy, 2019; Lev et al., 2019: Ouvang et al., 2019), suggesting that P granules are crucial for the maintenance of RNA homeostasis. The intrinsically disordered protein MUT-16 functions as a scaffold and promotes phase separation of *Mutator* foci, the depletion of which blocks the production of Mutator class siRNAs and results in defects in fertility (Phillips et al., 2012; Uebel et al., 2018; Zhang et al., 2011). Another intrinsically disordered protein, PID-2/ ZSP-1, which was reported to be needed for Z granule homeostasis, is required for heritable piRNA-induced silencing and germline immortality (Placentino et al., 2021; Wan et al., 2021). Our recent works identified the E granule as a novel subcompartment of C. elegans germ granules and revealed that both the PICS/ PETISCO complex (PICS-1/TOFU-6/PID-1/ERH-2) and the EGO complex (ELLI-1/EGC-1/EGO-1/DRH-3/EKL-1) are enclosed in the E granule (Chen et al., 2024; Huang et al., 2025; Zeng et al., 2019). The PICS complex is required for piRNA processing to produce mature piRNAs (Cordeiro Rodrigues et al., 2019; Zeng et al., 2019), and the EGO complex is required for the generation of a specialized subset of siRNAs (Chen et al., 2024; Gu et al., 2009; Maniar and Fire, 2011). Yet, the cellular function of the perinuclear positioning of these two complexes is largely unknown. Identification of proteins that mediate E granule assembly and deciphering the E granule assembly process may help reveal how E granules coordinate multiple biological processes.

In this study, we utilized TurboID enzyme-catalyzed proximity labeling technology to identify additional components of the E granule in *C. elegans* germline. This approach led to the identification of 139 candidate proteins potentially localized to E granules. Through an RNAi-based reverse genetic screen, we successfully identified two uncharted proteins, C27B7.5/EGC-2 (E granule component-2) and F59G1.8/EGC-3 (E granule component-3), which facilitate the perinuclear localization of both the PICS and the EGO complexes. We demonstrated that

these proteins are enclosed in the E granule and exclusively promote E granule assembly. We further performed small RNAomic analyses and revealed that both EGC-2 and EGC-3 promote the production of 5' E-class siRNA, whereas piRNA accumulation is inhibited by EGC-3. Additionally, we found that EGC-2 and EGC-3 contribute to the RNAi response. Taken together, our results identify key factors involved in E granule assembly that are essential for maintaining small RNA homeostasis, and suggest that intracellular condensation may exert distinct regulatory effects on different biological processes.

RESULTS

The perinuclear accumulation of the EGO complex and PICS complex is independent of each other

The current model posits that the *C. elegans* germ granule is composed of multiple subcompartments (Figure 1A) (Huang et al., 2025; Phillips et al., 2022; Sundby et al., 2021). In previous studies, we identified a novel germ granule compartment, the E granule, which encloses the EGO complex (consisting of ELLI-1, EGC-1, EGO-1, EKl-1, and DRH-3) and the PICS complex (consisting of PICS-1, TOFU-6, PID-1, and ERH-2) (Figure 1B) (Andralojc et al., 2017; Chen et al., 2024; Huang et al., 2025; Zeng et al., 2019).

We previously found that ELLI-1 and EGC-1 are essential for the perinuclear accumulation of the EGO module (comprising EGO-1. EKL-1. and DRH-3) (Chen et al., 2024). We further investigated which components of the EGO complex may play the most upstream role in their perinuclear accumulation by examining whether the EGO module factors promote the perinuclear accumulation of ELLI-1 or EGC-1. Feeding RNAi targeting eqo-1 likely reduced the expression level of ELLI-1::GFP. vet a considerable number of ELLI-1 foci can still be observed in germ cells; RNAi knockdown of ego-1 completely disrupted perinuclear EGC-1 foci, suggesting that EGO-1 is required for the perinuclear accumulation of EGC-1 (Figure S1A); the DRH-3 foci and EKL-1 foci were also significantly disrupted upon ego-1 knockdown, and the residual foci of DRH-3 and EKL-1 colocalized with tagRFP::MUT-16 (Figure S1B and C). DRH-3 and EKL-1 form RdRP-modules with either RRF-1 or EGO-1, which function in multiple 22G-RNA pathways (Billi et al., 2014; Chen et al., 2024; Gu et al., 2009). In pachytene cells in the germline, EGO-1 is enriched in the E granule and RRF-1 is enriched in Mutator foci (Chen et al., 2024; Uebel et al., 2018). We previously found that both EKl-1 and DRH-3 accumulate in the E granule in early/ middle pachytene cells (Chen et al., 2024). The depletion of EGO-1 increases a subset of 22G RNAs, which largely belongs to the M-class 22G RNAs (Figure S1D), suggesting that the colocalization of DRH-3 and EKL-1 with MUT-16 foci in early/middle pachytene cells upon ego-1 knockdown may enhance the production of a subset of Mutator foci derived 22G RNAs. The knockdown of DRH-3 via an auxin-inducible degron system also elicited the diffusion of both EGC-1 and EGO-1 in germ cells, yet did not affect the perinuclear enrichment of ELLI-1 (Figure S1A) (Zhang et al., 2015). Together, these results suggest that ELLI-1 plays the most upstream role in the assembly of the EGO complex in E granules.

The PICS/PETISCO complex, which stabilizes the PUCH complex and facilitates 5' trimming of piRNA precursors, was enriched in the E granule (Huang et al., 2025; Podvalnaya et al.,

2023). We examined whether the EGO complex components, ELLI-1 and EGO-1, are required for the E granule accumulation of the PICS complex as well. Strikingly, RNAi knockdown of *elli-1* and *ego-1* did not disrupt the formation of the PICS foci (Figure 1C). The PICS foci disassembled in the absence of *pics-1* or *tofu-6* (Zeng et al., 2019). RNAi knockdown of *pics-1* or *tofu-6* disrupted the perinuclear foci of ERH-2, yet did not affect the formation of the EGO complex foci (Figure 1D).

Taken together, the results suggested that the perinuclear accumulation of the EGO and PICS complexes was likely independent of each other, hinting at the presence of certain master organizers that may act upstream to assemble E granules.

Identification of E granule components via TurboID-based proximity labeling

To identify additional proteins that promote E granule assembly, we sought to investigate the protein components of E granules. TurboID is an engineered biotin ligase that uses ATP to convert biotin into biotin-AMP, a reactive intermediate that covalently labels proximal proteins in living cells (Branon et al., 2018; Cho et al., 2020; Price et al., 2021; Wang et al., 2025) (Figure 2A). We then employed the biotin ligase-based proximity labeling method to label E granule proteins in this study. Since ELLI-1 plays the most upstream role in the assembly of the EGO complex in E granules (Chen et al., 2024), we used CRISPR/Cas9 to introduce the TurboID sequence into the genomic loci of *elli-1* (Figure S2A). The insertion of the TurboID sequence was confirmed by genotyping via PCR and DNA sequencing (Figure S2B)

We first assessed if the tagged *elli-1* allele generates functional proteins by examining the feeding RNAi response of animals expressing ELLI-1::TurboID proteins. Loss of ELLI-1 results in defects in feeding RNAi responses targeting germline genes (Chen et al., 2024). Compared with wild-type animals, animals expressing ELLI-1::TurboID proteins responded normally to feeding RNAi targeting *pos-1* and *mex-3* (Figure S2C and D). To determine whether E granules are normally assembled in the *elli-1::TurboID* strain, we examined the subcellular localization of EGC-1, a well-characterized E granule protein (Chen et al., 2024). Like in wild-type animals, EGC-1::GFP primarily accumulated in perinuclear foci in *elli-1::TurboID* animals (Figure S2E). Together, the results suggest that the modified *elli-1* gene encodes functional proteins.

To assess the catalytic activity of TurboID, we next examined the biotinylation of proteins via immunofluorescence staining of dissected gonads and streptavidin blot analysis of whole-animal lysate. Firstly, we stained and dissected gonads with fluorescently labeled streptavidin to examine the cellular localization of biotinylated proteins in germ cells. Cytoplasmic signals were barely detectable in the stained wild-type gonads, whereas pronounced perinuclear signals of biotinylated proteins were observed in *elli-1::TurboID* gonads (Figure 2B). Streptavidin–horseradish peroxidase blot analysis of lysed adult animals further revealed a dramatically increased presence of biotinylated proteins in *elli-1::TurboID* samples compared with untagged control samples (Figure S2F). These results suggested that ELLI-1::TurboID can be applied to label proteins in living germ cells.

We next conducted streptavidin affinity pull-down assays to enrich TurboID-biotinylated proteins. Blotting results confirmed that biotinylated proteins were efficiently enriched in the pull-

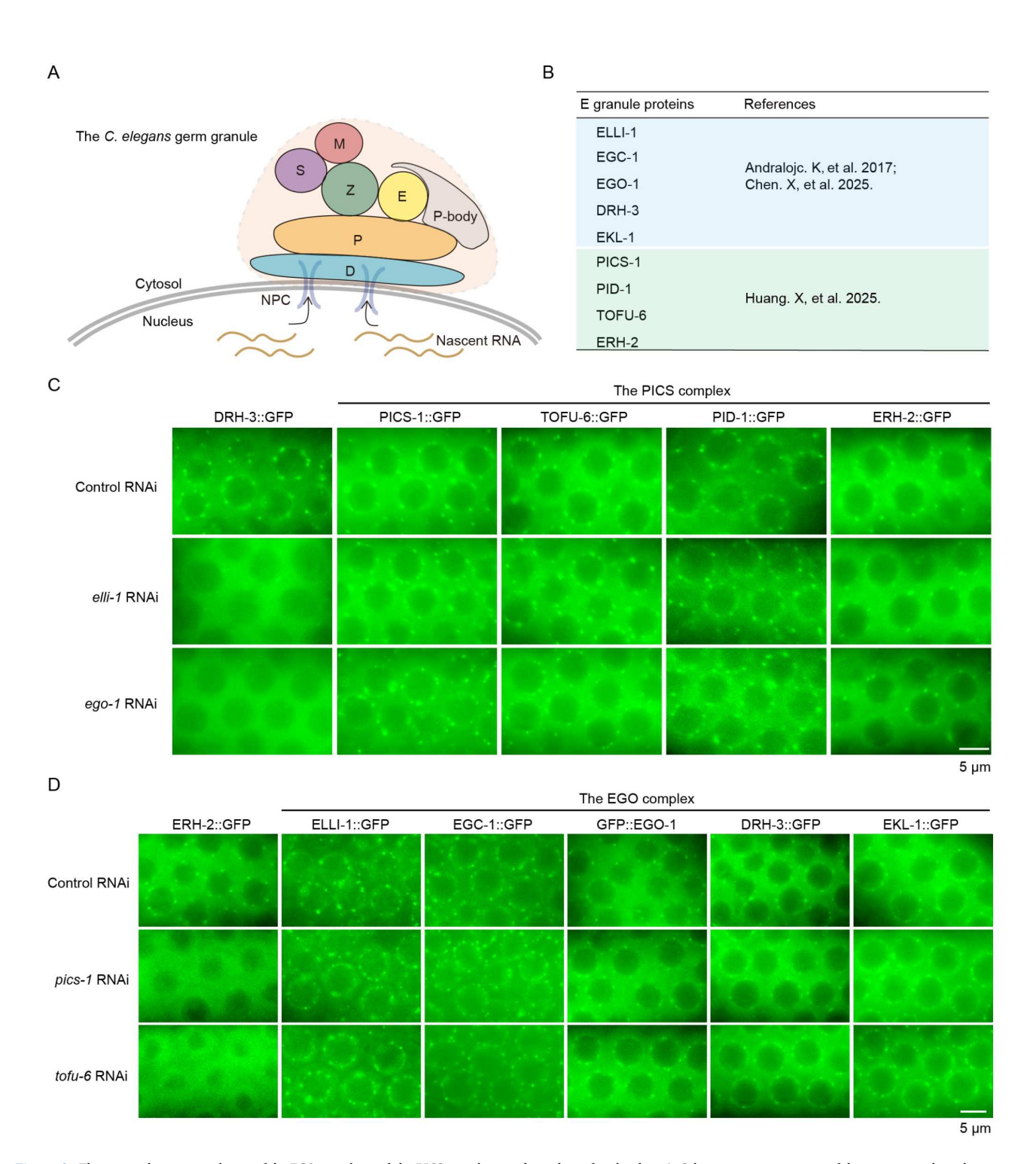


Figure 1. The perinuclear accumulation of the EGO complex and the PICS complex is independent of each other. A, Schematic representation of the germ granule architecture in *C. elegans* pachytene cells. Note, this model roughly shows the shapes and spatial organization of different germ-granule compartments. The precise spatial organization of each subcompartment within germ granules is still largely unknown. B, Summary of nine known E granule components. C, Fluorescence microscopy of the GFP-tagged PICS complex components in adult germ cells following RNAi targeting *elli-1* and *ego-1*. RNAi knockdown of *elli-1* and *ego-1* disrupted DRH-3::GFP foci, whereas PICS complex localization remained generally unaffected. D, Fluorescence micrographs of the GFP-tagged EGO complex components in adult germ cells following RNAi targeting *tofu-6* and *pics-1*. RNAi knockdown of *tofu-6* and *pics-1* destroyed the formation of ERH-2::GFP foci but did not disturb the perinuclear localization of the EGO complex. All images are representative of more than three animals.

down samples, with only minimal endogenously biotinylated proteins remaining in the flow-through samples (see methods) (Figure 2C). Biotinylated proteins from the untagged control and *elli-1::TurboID* strains were enriched, respectively, and were

identified via mass spectrometry. Mass spectrometry analysis revealed that 139 proteins were enriched in the ELLI-1::TurboID samples compared with the untagged sample (fold change of unique peptide counts≥3) (Figure 2D; Table S1). The candidate

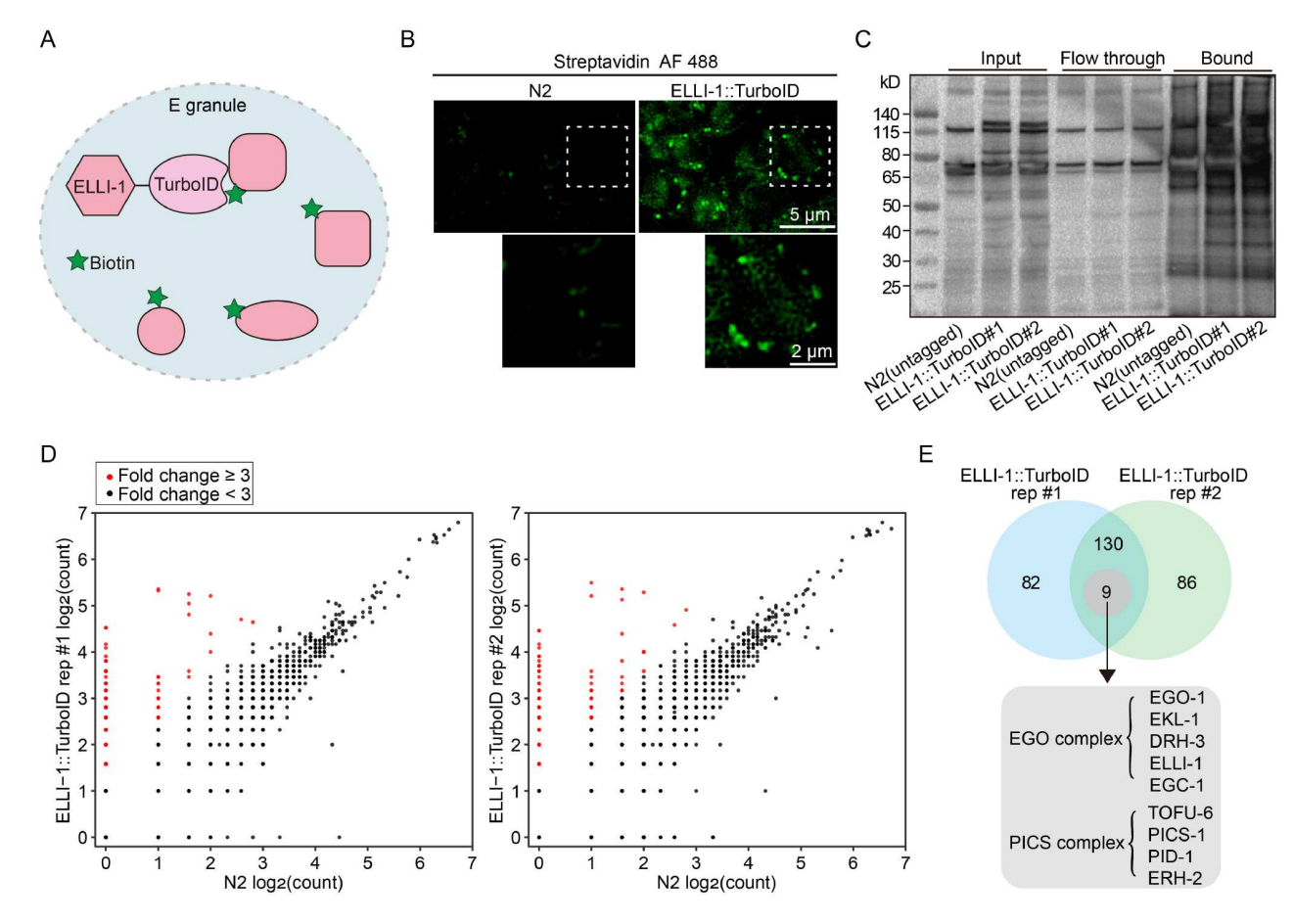


Figure 2. Identification of E granule proteins via TurboID-based proximity labeling. A, Schematic of proximity-based labeling in the E granule. The E granule protein ELLI-1 is tagged with the biotin ligase—TurboID—to label proteins present in E granules with biotins. B, Fluorescence micrographs of streptavidin-Alexa Fluor 488-stained germ cells from untagged N2 and elli-1::TurboID animals. C, Streptavidin affinity pull-down efficiency shown by streptavidin-HRP blotting. Biotinylated proteins from untagged animals (n=1) and elli-1::TurboID animals (n=2) were extracted from the input (seemethods), showing enrichment in the pull-down fraction, with minimal endogenously biotinylated proteins detected in the flow-through. D, Scatter plots showing the fold changes in unique peptide counts derived from mass spectrometry data, comparing elli-1::TurboID (n=2) to untagged animals (n=1), with a pseudocount of 1 to accommodate zeros. Proteins with a fold change $\geqslant 3$ (indicated by red dots) were artificially classified as putative E granule components, whereas those with a fold change $\leqslant 3$ are shown as black dots. E, Venn diagram showing 139 proteins identified in both TurboID-based proximity labeling replicates, including components of the EGO and PICS complexes.

list included all known components of the EGO complex (ELLI-1, EGC-1, EGO-1, DRH-3, and EKL-1) and the PICS complex (TOFU-6, PID-1, PICS-1, and ERH-2), suggesting that TurboID proximity labeling is effective for identifying proteins within E granules (Figure 2E).

Candidate-based RNAi screening identifies two proteins, EGC-2 and EGC-3, that promote the formation of perinuclear EGO foci and PICS foci. As membraneless organelles, E granules may constantly exchange internal substances with other germ granule compartments or with the cytosol. Thus, the TurboID technique may not only label proteins in E granules, but also label proteins enriched in the cytosol or in other germ granule compartments which are adjacent to E granules. To identify bona fide E granule components involved in E granule assembly, we then performed RNAi-based reverse genetic screening to identify proteins that facilitate the formation of perinuclear ELLI-1 foci. From the 139 candidate proteins, we first reduced the list by excluding proteins that were reported not to be enriched in the germline or localized to particular germ granule compartments other than the E granule (Harris et al., 2020; Huang et al., 2025), and obtained a narrowed list that consists of 40 proteins.

We then separately knocked down these 40 genes in *elli-1::gfp* animals by feeding them bacteria expressing corresponding dsRNAs to determine whether the depletion of these genes disrupted ELLI-1 foci formation (Figure 3A). Two genes, c27b7.5 and f59g1.8, were identified as essential genes for ELLI-1 foci formation (Figure 3B). Based on the data described below, c27b7.5 and f59g1.8 were named E granule component-2 (*egc-2*) and E granule component-3 (*egc-3*), respectively.

To further confirm that EGC-2/C27B7.5 and EGC-3/F59G1.8 promote ELLI-1 foci assembly, we generated mutant alleles of *egc-2* and *egc-3* via multiple sgRNAs guided CRISPR/Cas9 technology (Figure S3) (Chen et al., 2014). Using genetic crosses, we generated *egc-2*(–) and *egc-3*(–) animals expressing ELLI-1::GFP. Consistent with the RNAi results, ELLI-1 foci were significantly disrupted in these mutant animals (Figure 3C and D). Together, these results suggest that both EGC-2 and EGC-3 are required for ELLI-1 foci formation in germ cells.

Next, we examined whether EGC-2 and EGC-3 are required for the perinuclear localization of other components of the EGO and PICS complexes. In both *egc-2* and *egc-3* mutants, the perinuclear foci of EGC-1, TOFU-6, PICS-1, and ERH-2 were all eliminated

	Foci of		Foci of		Foci of		Foci of		Foci of
Gene ID	ELLI-1::GFP	Gene ID	ELLI-1::GFP	Gene ID	ELLI-1::GFP	Gene ID	ELLI-1::GFP	Gene ID	ELLI-1::GFP
xrn-1	+	sams-3	+	mdt-4	+	W05F2.6	+	M04B2.4	+
let-716	+	natc-1	+	Y66D12A.1	19 +	F56C9.6	+	F13D12.5	+
rha-1	+	lea-1	+	gyf-1	+	eftu-2	+	T05F1.2	+
mog-4	+	H05C05.1	+	frm-4	+	F01G4.4	+	cpb-3	+
dcap-1	+	T23H2.3	+	smn-1	+	cey-2	+	ife-2	+
C27B7.5	-	hcp-1	+	F46F11.1	+	F59G1.8	-	Y66D12A.1	6 +
D2005.4	+	T21B10.3	+	mask-1	+	mina-1	+	eef-1B.2	+
sna-2	+	cey-3	+	atx-2	+	F07H5.10	+	Y54E2A.4	+

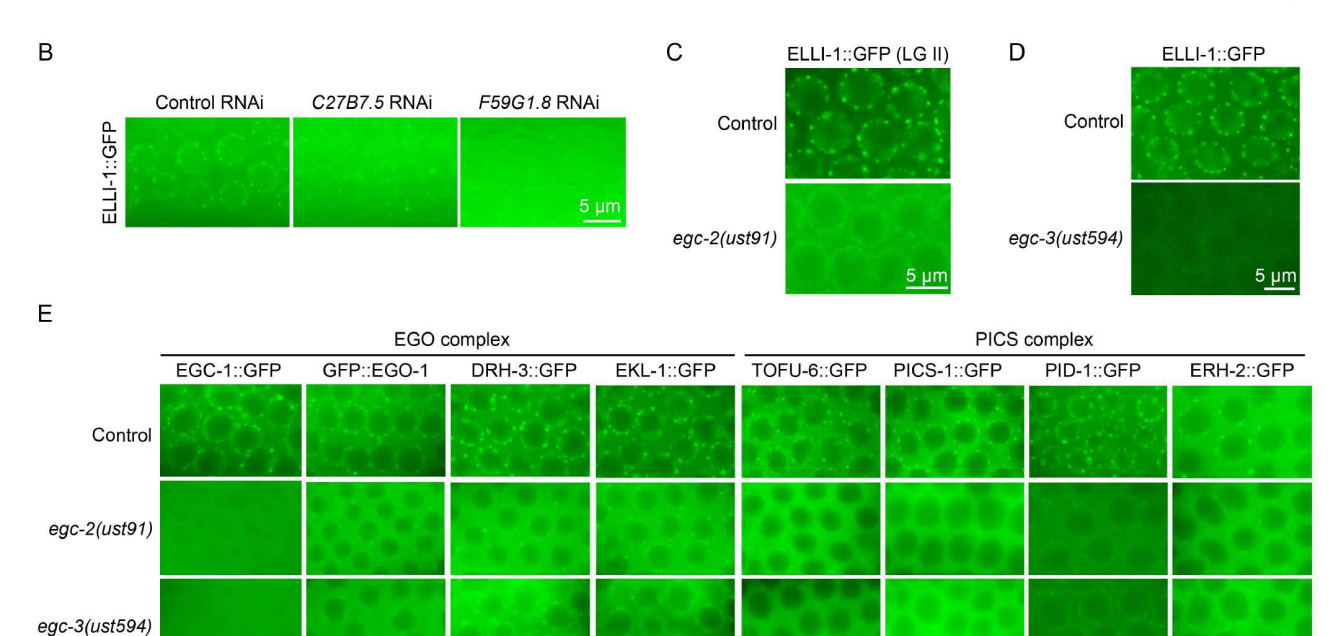


Figure 3. Candidate-based RNAi screening identifies two proteins, EGC-2/C27B7.5 and EGC-3/F59G1.8, that promote the formation of perinuclear EGO foci and PICS foci. A, A summary table listing 40 candidate genes evaluated via RNAi-based reverse genetic screening. The impact on ELLI-1::GFP foci was assessed by feeding RNAi targeting these candidates; "-" denotes the disruption of ELLI-1::GFP foci, whereas "+" indicates no effect. B, Fluorescence micrographs of ELLI-1::GFP in pachytene germ cells upon RNAi targeting C27B7.5 and F59G1.8. C and D, Pachytene germ cells from dissected gonads expressing ectopic ELLI-1::GFP (LG II) (C) or in situ ELLI-1::GFP (LG IV) (D) in the indicated animals. As C27B7.5(LG IV, 4.00 cM) and elli-1(ust354[elli-1::gfp::3xflag]) (LG IV, 3.96 cM) are genetically linked, an ectopically expressed ELLI-1::GFP transgene (ust1S268, LG II, 0.77 cM) was used (C). E, Fluorescence micrographs of the GFP-tagged components of the EGO and PICS complexes in the adult germlines of egc-2(-) and egc-3(-) animals. The loss of EGC-2 or EGC-3 resulted in the disruption of perinuclear localization of both the EGO and the PICS complexes. All images are representative of more than three animals.

(Figure 3E). The perinuclear foci of PID-1 were also substantially disrupted in *egc-2* and *egc-3* mutants, although few perinuclear PID-1 aggregates remained observable (Figure 3E). The localization of EGO module factors (EGO-1, DRH-3, and EKL-1) to perinuclear foci was significantly reduced in both *egc-2*(–) and *egc-3*(–) animals; however, residual EGO module-marked foci were still noticeable (Figure 3E). These results suggest that EGC-2 and EGC-3 are required for perinuclear localization of both the EGO and PICS complexes.

EGC-2 and EGC-3 are enriched in the E granule and promote E granule assembly

The assembly of biomolecular condensates is generally driven by intrinsically disordered/low-complexity proteins (Banani et al., 2017). Both EGC-2 and EGC-3 possess low-complexity domains, hinting that these proteins might facilitate E granule assembly (Figure S4A and B) (Erdős and Dosztányi, 2024). To investigate

the expression patterns and subcellular localization of EGC-2 and EGC-3, we constructed a single-copy qfp::3xflaq-tagged eqc-2 transgene using the MosSCI system (Frøkjær-Jensen et al., 2008) and introduced a gfp::3xflag epitope into the endogenous egc-3 gene via CRISPR/Cas9 technology (Huang et al., 2025). Ectopically expressed EGC-2 transgenes tagged with 3xFLAG:: GFP largely rescued the decline in fertility of egc-2(-) animals (Figure S4C). Animals carrying the tagged egc-3 gene produce a normal number of progeny and are responsive to feeding RNAi at similar levels to those of wild-type animals (Figure S4D and E). These results suggest that the tagged proteins largely recapitulate the endogenous functions of these proteins. Both of these proteins were expressed throughout the germline and predominantly accumulated in perinuclear foci in germ cells, similar to other E granule proteins (Figure S4F) (Chen et al., 2024). Yet, unlike previously reported E granule proteins (Chen et al., 2024), EGC-2 and EGC-3 were expressed and enriched mainly in cytoplasmic condensates in early embryos, implying that EGC-2 and EGC-3

may exercise cellular functions independent of the PICS and EGO complexes during embryogenesis (Figure S4G).

To assess whether EGC-2 and EGC-3 localize to the E granule, we used genetic crosses to generate animals expressing combinations of tagRFP::ELLI-1 and EGC-2::GFP or EGC-3::GFP. We found that both EGC-2::GFP and EGC-3::GFP colocalized with tagRFP::ELLI-1 (Figure 4A and B). Moreover, the visualization of the endogenous EGC-2 protein via utilizing a split-GFP approach also supported that EGC-2 colocalized with ELLI-1 (Figure S4H) (Goudeau et al., 2021). Together, these results suggested that both EGC-2 and EGC-3 localize to the E granule.

We further examined whether the PICS and EGO complexes regulate the formation of perinuclear EGC-2::GFP and EGC-3:: GFP foci. The perinuclear EGC-2 foci were largely unaffected upon knockdown of pid-1(-) or in egc-3(-) animals (Figure 4C and D); the depletion of ELLI-1 and PID-1 did not disrupt EGC-3 foci either (Figure 4E). Additionally, in pachytene germ cells, the perinuclear localization of EGC-2 and EGC-3 was disrupted in each other's mutants. Interestingly, EGC-3 is also required for the formation of EGC-2::GFP foci in early embryos (Figure S5A), whereas the depletion of EGC-2 did not destroy embryonic EGC-3::GFP condensates (Figure S5B), implying distinct molecular mechanisms of E granule assembly at different developmental stages. Meanwhile, the components of both the PICS and EGO complexes largely diffused in the cytosol in early embryos and reaggregate in E granules in L1 animals (Chen et al., 2024; Zeng et al., 2019), suggesting that the protein components of particular condensates may vary during development. Together, these results suggested that both EGC-2 and EGC-3 function upstream of other E granule components in E granule assembly, and their perinuclear localization is mutually dependent.

The current model posits that *C. elegans* germ granules in pachytene cells consist of at least seven subcompartments. Thus, we examined whether EGC-2 and EGC-3 participate in the assembly of other germ granule compartments. Genetic crosses were performed to generate *egc-2* and *egc-3* mutant animals expressing fluorescent markers for each subcompartment. The results showed that the mutations specifically affected E granule assembly, without disrupting the formation of P granules (marked by PGL-1::GFP), Z granules (marked by GFP::ZNFX-1), SIMR foci (marked by SIMR-1::tagRFP), *Mutator* foci (marked by mCherry::MUT-16), D granules (marked by DDX-19::tagRFP), or P-bodies (marked by mCherry::CGH-1) (Figure 4F).

Overall, these results reveal that EGC-2 and EGC-3 are dedicated E granule components that exclusively promote E granule assembly, with no detectable impact on the formation of other germ granule subcompartments.

EGC-2 and EGC-3 promote the production of 5' E-class siRNA

Previous studies have shown that EGC-1 and ELLI-1, which facilitate perinuclear accumulation of the EGO module, are essential for 5' E-class siRNA production (Chen et al., 2024). We then investigated whether EGC-2 and EGC-3 also play a role in 5' E-class siRNA generation. We extracted total RNA from wild-type, egc-2(–) and egc-3(–) animals, performed 5' phosphate-dependent small RNA sequencing. 22G RNAs were mapped to the *C. elegans* genome, and the number of siRNAs complementary to each *C. elegans* germline gene was quantified. E-class siRNAs were generally reduced in both egc-2 and egc-3 mutants,

although the reduction of siRNAs in *egc-2* mutants was less pronounced than that in *egc-3* mutants (Figure 5A and B; Figures S6A and S7A).

The E-class siRNAs reduced in *egc-2* mutants were predominantly mapped to the 5′ portion of the E-class genes. For instance, in wild-type animals, siRNAs targeting *klp-7*, *cls-2*, *FO1G4.4*, *tebp-2*, *csr-1*, and *hcp-1* were evenly distributed across the length of their target mRNAs (Figure 5C; Figure S6B). However, in *egc-2* mutants, siRNAs mapping to the 5′ portions were generally reduced by more than half, whereas 3′ end siRNAs remained relatively unaffected (Figure 5C; Figure S6B). Metagene analysis of 22G RNAs along E-class genes showed that the siRNAs mapping to the 5′ portion, but not the 3′ end siRNAs, of E-class genes was decreased in *egc-2* mutants (Figure 5D). EGC-2 was not required for the production of M-class siRNAs, which are dependent on the *Mutator* protein, MUT-16 (Figure S6C and D).

In *egc-3* mutants, the reduction of E-class siRNAs mapping to E-class genes was even more significant than in *egc-2* mutants, resembling the effects observed in *egc-1* and *elli-1* mutants (Chen et al., 2024). For example, siRNAs mapping to the 5' portions of *klp-7*, *cls-2*, *F01G4.4*, *tebp-2*, *csr-1*, and *hcp-1* mRNAs were almost entirely absent, whereas 3' end siRNAs remained largely unaffected in *egc-3* mutants (Figure 5E; Figure S7B). Metagene analysis showed a substantial loss of siRNAs mapping to the 5' portions of E-class genes in *egc-3*(–) animals, whereas 3' end siRNAs also remained unaffected (Figure 5F). Like EGC-2, EGC-3 was not involved in M-class siRNA production (Figure S7C and D). These results suggest that while EGC-3 plays a role in E granule assembly, it might also participate in the amplification of siRNAs along E-class mRNAs (see discussion).

E granule components exert multiple regulatory effects on piRNA accumulation

The PICS/PETISCO complex engages in piRNA processing, the depletion of which blocks the production of mature piRNAs (Cordeiro Rodrigues et al., 2019; Zeng et al., 2019). Since the components of the PICS complex are all enriched in the E granule and their perinuclear localization requires both EGC-2 and EGC-3, we then examined whether the localization of the PICS complex in the germ granule is essential for piRNA processing.

We extracted total RNA from wild-type, egc-2(–) and egc-3(–) animals, performed 5′ phosphate-dependent small RNA sequencing, and quantified each piRNA. The 5′ phosphate-dependent small RNA sequencing method excludes secondary siRNA signals that have 5′ triphosphate ends, and thus boosts the relative piRNA signals in the sequencing results. Surprisingly, the accumulation of mature piRNAs remained largely unchanged upon the loss of EGC-2 (Figure 6A and B; Figure S8A–C), suggesting that the localization of the PICS complex in E granules may not be necessary for piRNA processing (see discussion).

Interestingly, piRNA expression levels were significantly elevated in *egc-3*(–) animals, suggesting a potential role for EGC-3 in limiting piRNA production (Figure 6C and D; Figure S8D–H). We further evaluated the activity of the piRNA-mediated germline surveillance pathway in *egc-3* mutants via a piRNA sensor assay. The current model posits that piRNAs mediate the genome-wide surveillance of germline transcripts to silence non-self RNA transcripts in *C. elegans* (Ashe et al., 2012; Lee et al., 2012; Luteijn et al., 2012; Shirayama et al., 2012). In wild-type animals, the GFP-labeled piRNA sensor transgene is

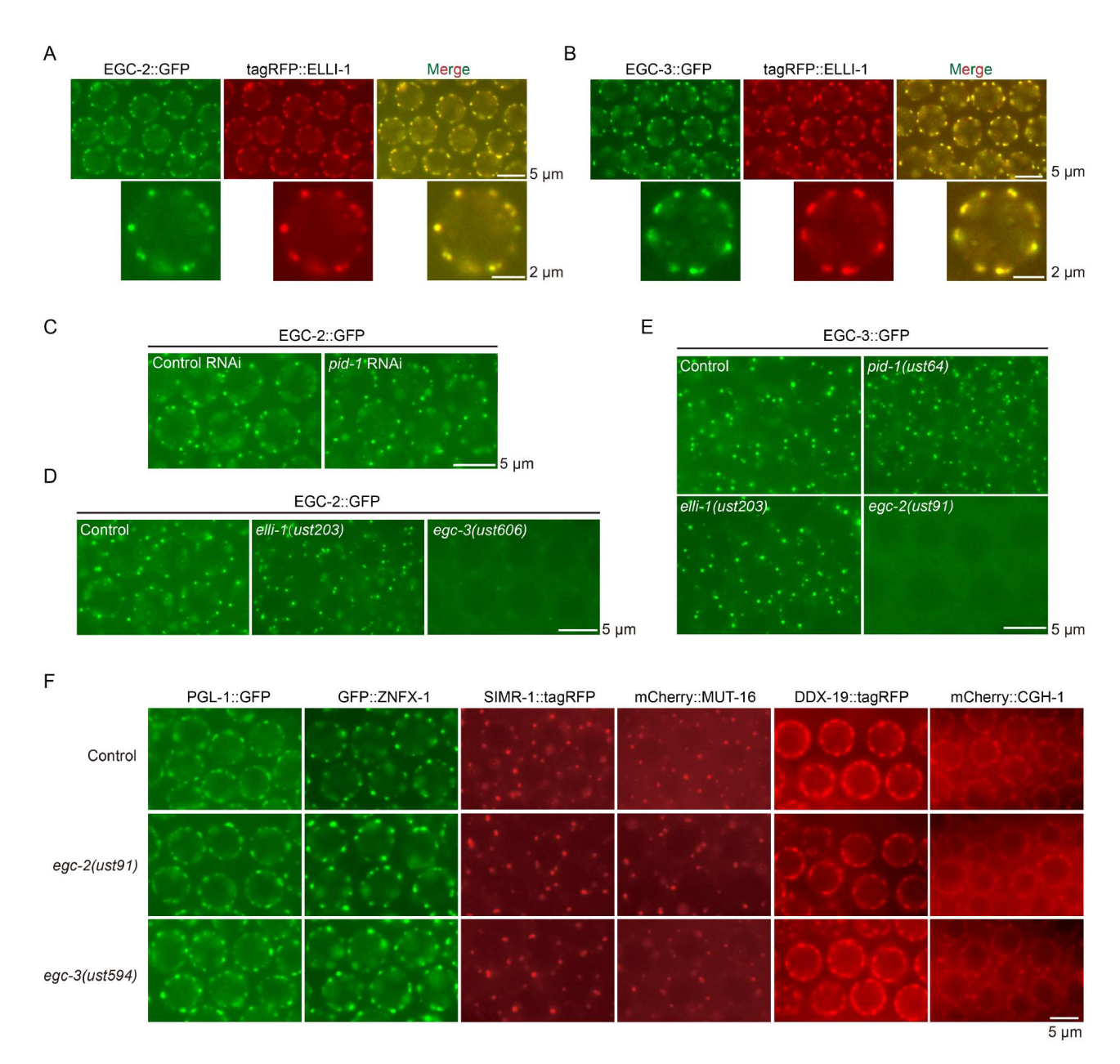


Figure 4. EGC-2 and EGC-3 are enriched in the E granule and promote E granule assembly. A and B, Fluorescence micrographs of pachytene germ cells expressing the indicated fluorescent proteins. Both EGC-2::GFP (A) and EGC-3::GFP (B) colocalized with tagRFP::ELLI-1. C and D, Fluorescence micrographs of EGC-2::GFP in pachytene germ cells upon pid-1 RNAi treatment (C) or in indicated animals (D). Since pid-1(LG II, 0.52 cM) and the ectopically expressed EGC-2::GFP transgene (ustSi57, LG II, 0.77 cM) are closely linked, pid-1 RNAi treatment was conducted to knock down its expression level in the EGC-2::GFP animals (C). The depletion of PID-1 or ELLI-1 did not disturb the perinuclear localization of EGC-2 or EGC-3; the depletion of EGC-2 and EGC-3 mutually disrupted each other's perinuclear localization. E, Fluorescence micrographs of EGC-3::GFP in the indicated animals. F, Fluorescence micrographs of adult germ cells expressing PGL-1::GFP (marking P granule), GFP::ZNFX-1 (marking Z granule), SIMR-1::tagRFP (marking SIMR foci), mCherry::MUT-16 (marking Mutator foci), DDX-19::tagRFP (marking D granule), or mCherry::CGH-1 (marking P body) in the indicated animals. Depletion of either EGC-2 or EGC-3 id not disturb the perinuclear localization of the other six germ granule subcompartments. All images are representative of more than three animals.

typically silenced and only reveals a weak fluorescent signal, but becomes desilenced when piRNA production is impaired or when piRNA-mediated gene silencing is disrupted (Bagijn et al., 2012; Cordeiro Rodrigues et al., 2019; Huang et al., 2021). TOFU-6 is required for piRNA production (Cordeiro Rodrigues et al., 2019; Zeng et al., 2019). RNAi-mediated depletion of TOFU-6 resulted in desilencing of the piRNA sensor (Figure S8I). Yet, knockdown of *egc-3* in the piRNA sensor strains further enhanced its silencing, further supporting that EGC-3 limits the production of piRNAs (Figure S8I).

Like EGC-3, a previous study has identified other E granule components, EGO-1 and EKL-1, as inhibitors of piRNA expression (Goh et al., 2014). Since EGO-1 and EKL-1 are all components of the EGO complex, we investigated whether other components of the EGO complex affect piRNA levels. We reanalyzed total small RNAs of ego-1(-), egc-1(-), and elli-1(-) animals from our published sequencing datasets (Chen et al., 2024) and sequenced the total small RNAs from drh-3::degron animals upon IAA treatment via a 5' phosphate-independent method. Consistent with the previous study, the depletion of EGO-1 results in

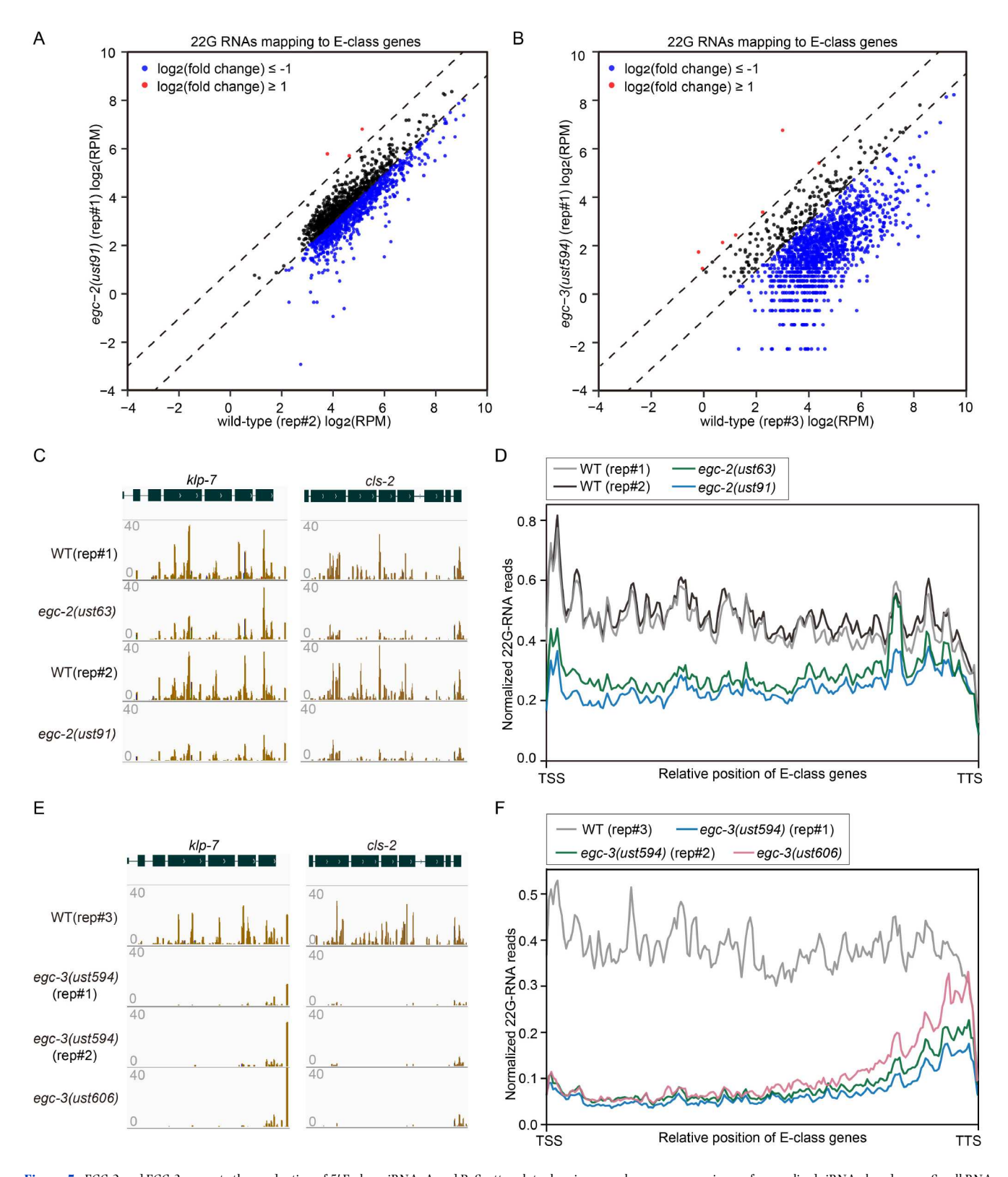


Figure 5. EGC-2 and EGC-3 promote the production of 5' E-class siRNA. A and B, Scatter plots showing gene-by-gene comparisons of normalized siRNA abundances. Small RNAs from indicated animals were sequenced via a 5' phosphate-independent method. Clean reads ranging from 17 to 30 nt were mapped to the *C. elegans* transcriptome assembly WS243. 22G RNAs were mapped to the *C. elegans* genome, and the number of reads complementary to each *C. elegans* gene was quantified. The number of total reads mapped to the transcriptome minus the number of total reads corresponding to sense ribosomal RNA (rRNA) transcripts (5S, 5.8S, 18S, and 26S) were used as the normalization number to exclude the possible degradation fragments of sense rRNAs. A cutoff criterion of a 2-fold change was applied to identify differentially expressed siRNAs. Genes with upregulated and downregulated siRNAs between wild-type and *egc-2(ust91)* animals (A) (*n*=2) or *egc-3(ust594)* animals (B) (*n*=2) are shown in red and blue, respectively. C and E, Normalized 22G RNA read distribution across E-class siRNAs targeting *klp-7* and *cls-2* in the indicated animals. Additional examples of E-class genes can be found in Figures S9 and S10. D and F, Metaprofile analysis showing the distribution of normalized 22G RNA reads (RPMs) along E-class genes in the indicated animals.

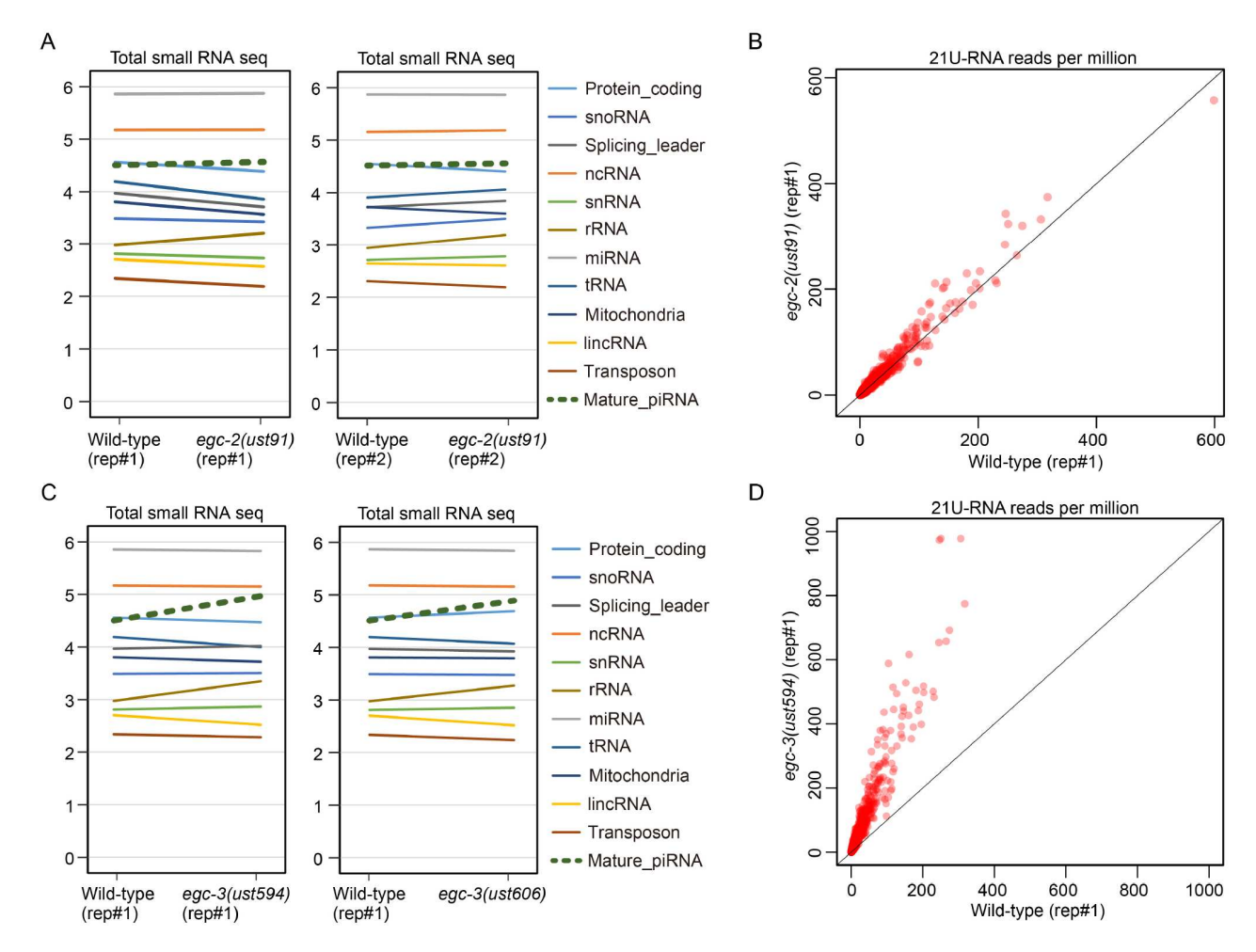


Figure 6. EGC-3, instead of EGC-2, prohibits piRNA production. A, Comparison of the abundance of small RNAs of different categories between wild-type and egc-2(-) animals (n=2) at the young adult stage. The blue dotted lines indicate piRNAs. Total small RNAs were extracted and deep-sequenced in a 5'-phosphate-dependent manner via an Illumina platform. Clean reads ranging from 17 to 35 nt were respectively mapped to mature piRNA regions, pre-piRNA regions, and the C. elegans transcriptome assembly WS243 using Bowtie2. The number of reads targeting each transcript was counted. The number of total reads mapped to the transcriptome minus the number of total reads corresponding to sense ribosomal RNA (rRNA) transcripts (5S, 5.8S, 18S, and 26S) were used as the normalization number to exclude the possible degradation fragments of sense rRNAs. piRNA expression was largely unchanged upon the loss of EGC-2. B, A scatterplot comparing the numbers of mature piRNA reads between animals in the indicated animals (n=2). C, Comparison of the abundance of small RNAs of different categories between wild-type and egc-3(p=4) (p=2) or egc-3(p=4) (p=1) animals. piRNA expression was significantly upregulated in egc-3(p-3) animals. p-1 animals. p-1 animals. p-1 animals. p-1 animals in the indicated animals (p=2).

dramatical upregulation of piRNAs (Figure S9A). Further analysis revealed that all other components of EGO complex, including EGC-1, ELLI-1, and DRH-3, inhibit piRNA accumulation, indicating that the EGO complex limits piRNA biogenesis in germ cells (Figure S9B–D). Consistently, knockdown of *elli-1* or *ego-1* by RNAi in germ cells resulted in further silencing of piRNA sensors (Figure S9E).

Together, these results suggest that different E granule components may exert multiple regulatory effects on piRNA accumulation, namely, the PICS complex promotes piRNA biogenesis, while EGC-3 and the EGO complex limit piRNA biogenesis, but possibly in an E granule-independent manner.

EGC-3 inhibits piRNA production via restraining the production of PRG-1 proteins

PRG-1 is the only member of the *C. elegans* PIWI family that exclusively binds to piRNAs and is essential for piRNA production (Batista et al., 2008; Das et al., 2008; Wang and Reinke, 2008).

EGO-1, CSR-1, and EKL-1 were reported to potentially act as piRNA suppressors by regulating the mRNA levels of prg-1 (the C. elegans piwi gene) (Goh et al., 2014), possibly in a siRNAdependent manner. We found that EGO-1 is essential for the production of the whole siRNAs mapping to the prg-1 mRNA (Figure 7A), and EGC-1, ELLI-1 and EGC-3 are required for the production of siRNAs targeting the 5' portion of prg-1 mRNA (Figure 7A and B), suggesting that siRNAs antisense to the prg-1 mRNA belong to the E-class siRNAs (Chen et al., 2024). To extend our understanding of the functions of EGC-3 and the EGO complex in regulating piRNA production, we examined the expression levels of prg-1 mRNA via mRNA deep sequencing and qRT-PCR. Consistent with a previous report (Goh et al., 2014), the mRNA level of prg-1 was dramatically increased in ego-1(-) animals (Figure 7C). In both egc-1 and elli-1 mutants, prg-1 mRNA levels were nearly doubled (Figure 7D and E). However, the level of prg-1 mRNAs was largely unchanged in the egc-3(-) animal (Figure 7F and G). Correspondingly, the mRNA level of rps-1, which does not belong to the E-class genes (Chen et al.,

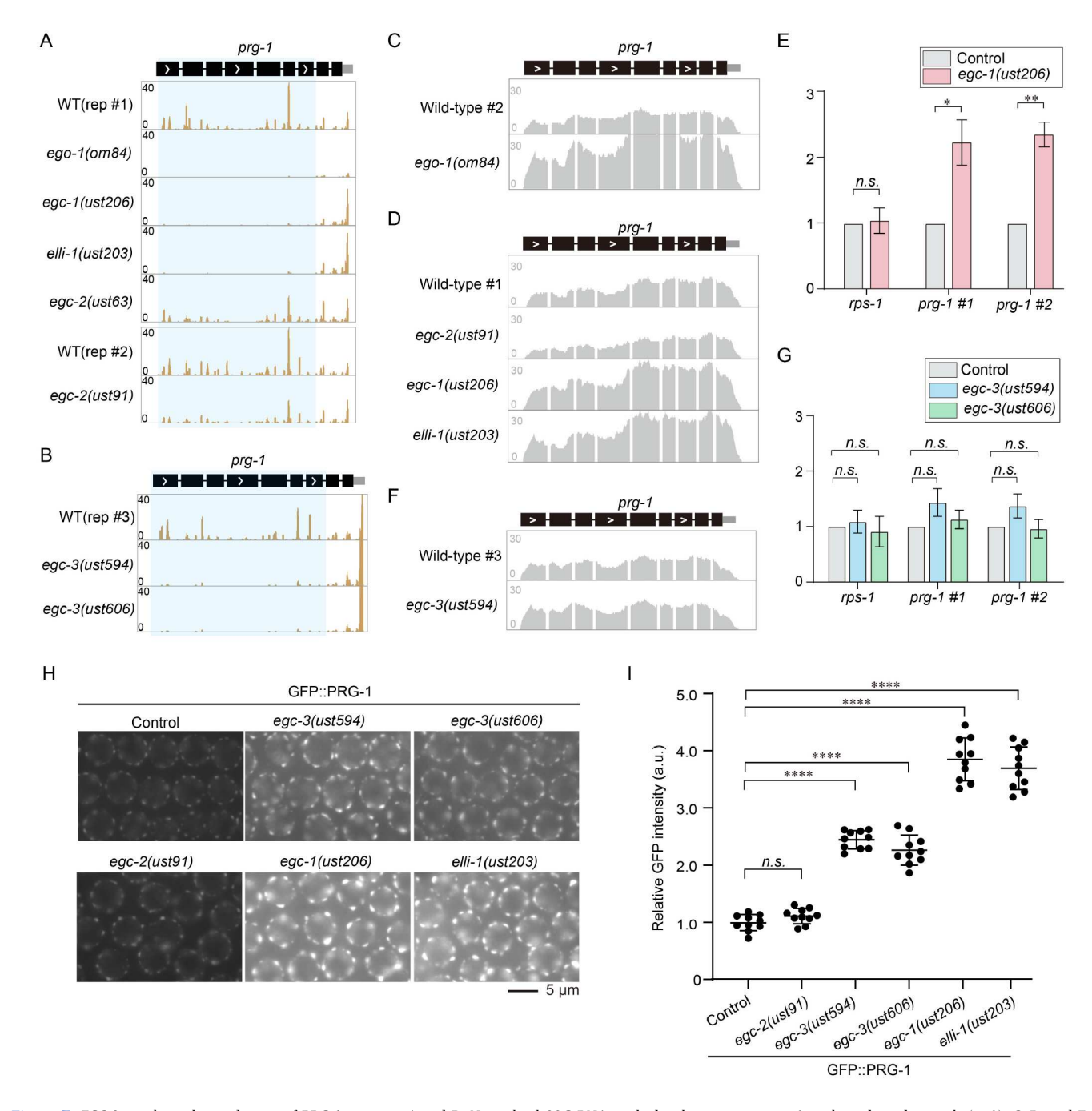


Figure 7. EGC-3 regulates the production of PRG-1 proteins. A and B, Normalized 22G RNA reads distribution across prg-1 in the indicated animals (n=1). C, D, and F, Normalized mRNA reads distribution along prg-1 in the indicated animals (n=1). E and G, Quantification of mRNA abundances by qRT-PCR in the indicated animals. Data are presented as the mean±SD of three biologically independent samples. Statistical analysis was performed via a two-tailed Student's t-test. n.s., not significant; *, P<0.01. H, Images of GFP::PRG-1 in the indicated animals. All images are representative of more than three animals. I, The quantification of GFP intensities of GFP::PRG-1 in the indicated animals. The relative GFP intensities were measured by ImageJ. Statistical analysis was performed with via a two-tailed Student's t-test. Mean±SD; *****, t<0.0001; t<0.0001; t<0.0001 animals.

2024), did not change in *ego-1*, *egc-1*, *elli-1*, and *egc-3* mutants (Figure S10A–C). These results suggested that EGC-3 may inhibit piRNA production, independent of regulating *prg-1* mRNA levels.

To further investigate how EGC-3 regulates piRNA production, we examined whether EGC-3 affects the synthesis of PRG-1 proteins by quantifying fluorescent signals of GFP::PRG-1 in *egc-3* mutants. Although the depletion of EGC-3 did not change the expression level of *prg-1* mRNAs, the protein level of PRG-1 dramatically increased upon the loss of EGC-3 (Figure 7H).

Similarly, *prg-1* mRNA levels were only doubled in both *egc-1* and *elli-1* mutants, but PRG-1 protein levels increased by nearly 4-fold in these mutants. These data implied that siRNAs targeting the 5' portion of *prg-1* mRNAs may regulate the translation efficiency of *prg-1* mRNAs.

Together, these results suggest that EGC-3 restrains the production of PRG-1 proteins without affecting *prg-1* mRNA levels. Since the production of siRNAs antisense to the 5' portion of *prg-1* mRNAs was blocked in *egc-3* mutants, we speculated

that these siRNAs may reduce the translation efficiency of *prg-1* mRNAs, yet the mechanism is unclear (see discussion).

EGC-2 and EGC-3 promote RNA interference

Given the roles of EGC-2 and EGC-3 in siRNA production, we then examined whether these proteins are required for RNAi response by feeding animals bacteria expressing dsRNAs targeting specific nematode genes. pos-1 encodes a zinc-finger protein that is required for early embryonic cell fate decision (Tabara et al., 1999). RNAi targeting pos-1 induces embryonic arrest in F1 embryos of animals exposed to dsRNA (Tabara et al., 1999). We fed the mutants with bacteria expressing dsRNAs targeting pos-1 and found that egc-3(-) animals exhibited resistance to pos-1mediated RNAi, whereas egc-2(-) animals responded similarly to wild-type animals (Figure 8A). Animals lacking EGC-3 were also defective for experimental RNAi targeting mex-3, which encodes a KH domain protein that regulates the development of early C. elegans embryos (Figure 8B) (Draper et al., 1996). We further tested the silencing efficiency of a germline-expressed gfp::h2b transgene upon gfp RNAi. We fed hatched animals bacteria expressing *qfp* dsRNA to induce exogenous RNAi targeting *h2b*:: gfp. In wild-type animals, RNAi targeting gfp results in silencing of h2b::gfp in 100% of gonads of P0 animals exposed to gfp dsRNA (Figure 8C). The loss of EGC-3 completely prohibited the silencing effect of GFP::H2B upon feeding RNAi targeting gfp (Figure 8C).

SID-1 and RDE-11 are required for dsRNA transportation and siRNA biogenesis during the RNAi response (Winston et al., 2002; Yang et al., 2012; Zhang et al., 2012). Recent studies reported that meg-3/4 animals produce aberrant siRNAs targeting sid-1 and rde-11, which silence the expression of these two genes and consequently result in defects in feeding RNAi response (Dodson and Kennedy, 2019; Lev et al., 2019; Ouvang et al., 2019). These two genes were also abnormally silenced in egc-1 and elli-1 mutants (Chen et al., 2024). We found that siRNAs targeting these two genes are dramatically upregulated in egc-3(-) animals (Figure S11A). We then conducted mRNAseq on wild-type and egc-3(-) animals to examine the expression levels of these two genes. As expected, sid-1 and rde-11 mRNA levels were dramatically downregulated in egc-3 mutants (Figure S11B and C). As a comparison, in the egc-2(-) animal, sid-1 and rde-11 siRNAs are unchanged, and the mRNA levels of these genes remained largely unaffected (Figure S11C-E). Thus, these data suggested that the silencing of the sid-1 and rde-11 genes may underlie the defect of egc-3(-) animals in exogenous RNAi.

Exogenous RNAi-induced gene silencing could be effectively inherited across multiple generations, even in the absence of continuous feeding of dsRNA to the offspring nematodes (Figure 8D) (Ishidate et al., 2018; Wan et al., 2018; Xu et al., 2018). Interestingly, although EGC-2 is not required for exogenous RNAi-induced gene silencing of *h2b::gfp* in P0 generation, *egc-2* (–) mutants exhibited a modest defect in the inheritance of RNAi in the offspring (Figure 8D). Together, these results suggest that EGC-2 and EGC-3 promote RNA interference in germ cells.

DISCUSSION

Here, via TurboID-based proximity labeling technology combined with RNAi-based genetic screening, we identify two novel intrinsically disordered proteins, EGC-2 and EGC-3, that are required for E granule formation and small RNA homeostasis.

The loss of EGC-2 or EGC-3 results in the disruption of the perinuclear localization of the EGO complex and the PICS complex. Both EGC-2 and EGC-3 were enriched in the E granule. Small RNAomics revealed that EGC-2 and EGC-3 promote the production of 5' E-class siRNA. Interestingly, although the loss of EGC-2 does not disturb the production of piRNAs, piRNAs are excessively accumulated in *egc-3*(–) animals. Moreover, EGC-3 is required for RNAi response, and EGC-2 promotes RNA inheritance. Together, we speculate that EGC-2 and EGC-3 are key nodes in the core interaction network of E granule assembly, and are crucial for maintaining the homeostasis of the E granule and the enclosed small RNAs.

E granule assembly and siRNA production

Biomolecular condensates are networks of protein-protein interactions and protein-RNA interactions, where high-valence scaffold proteins serve as central nodes that drive condensate formation. For example, G3BP proteins function as central nodes in stress granule (SG) assembly, exhibiting the highest centrality within the core SG network (Guillén-Boixet et al., 2020; Sanders et al., 2020; Yang et al., 2020). The interaction of G3BP with UBAP2L and Caprin-1 increases valency, facilitating liquid-liquid phase separation (LLPS) and subsequent SG formation (Hofmann et al., 2021). In this study, we identified two intrinsically disordered proteins, EGC-2 and EGC-3, as key players in E granule assembly. However, the molecular mechanisms underlying their roles in E granule assembly remain to be elucidated. Since the perinuclear localization of EGC-2 and EGC-3 is mutually dependent and the depletion of either protein disrupts the perinuclear localization of both the PICS and EGO complexes, we speculate that these two proteins may both function as central nodes or scaffold proteins during E granule assembly. Future studies will be necessary to validate this hypothesis, and approaches such as immunoprecipitation/mass spectrometry (IP/MS) to identify EGC-2 or EGC-3 interactors may provide further insights into the molecular mechanisms of E granule assembly.

In this study, we found that the biogenesis of 5' E-class siRNAs was significantly impaired in egc-2 or egc-3 mutants, and this loss was less pronounced in egc-2 mutants than in those lacking the EGO module or EGC-3, implying that concentrating RdRP machineries within the E granule may only improve the efficiency of siRNA amplification, rather that serving as a prerequisite for intracellular siRNA production. Thus, we proposed a model to illustrate our understanding of the role of E granules on siRNA amplification (Figure 9). In wild-type animals, 5' E-class siRNAs are produced in E granules. When the E granule was disrupted upon the loss of EGC-2, the EGO complex could still perform extension in the cytosol along targeted RNA transcripts, although with reduced efficiency. Therefore, the condensation of E granule components per se may be not essential for the generation of these siRNAs, but may enhance the efficiency of siRNA amplification (Figure 9). Alternatively, E granules may still form in *egc-2*(–) animals, albeit to a degree that may not be detectable via light microscopy. In elli-1 and eac-1 mutants, EGO modules (EGO-1/EKL-1/DRH-3) were incapable of performing the extension step of siRNA amplification, yet the initiation step for the biogenesis of siRNAs mapping to the 3' end regions of E class RNA transcripts might be unaffected in the cytosol (Figure 9). EGC-3 may facilitate the recruitment of E-class

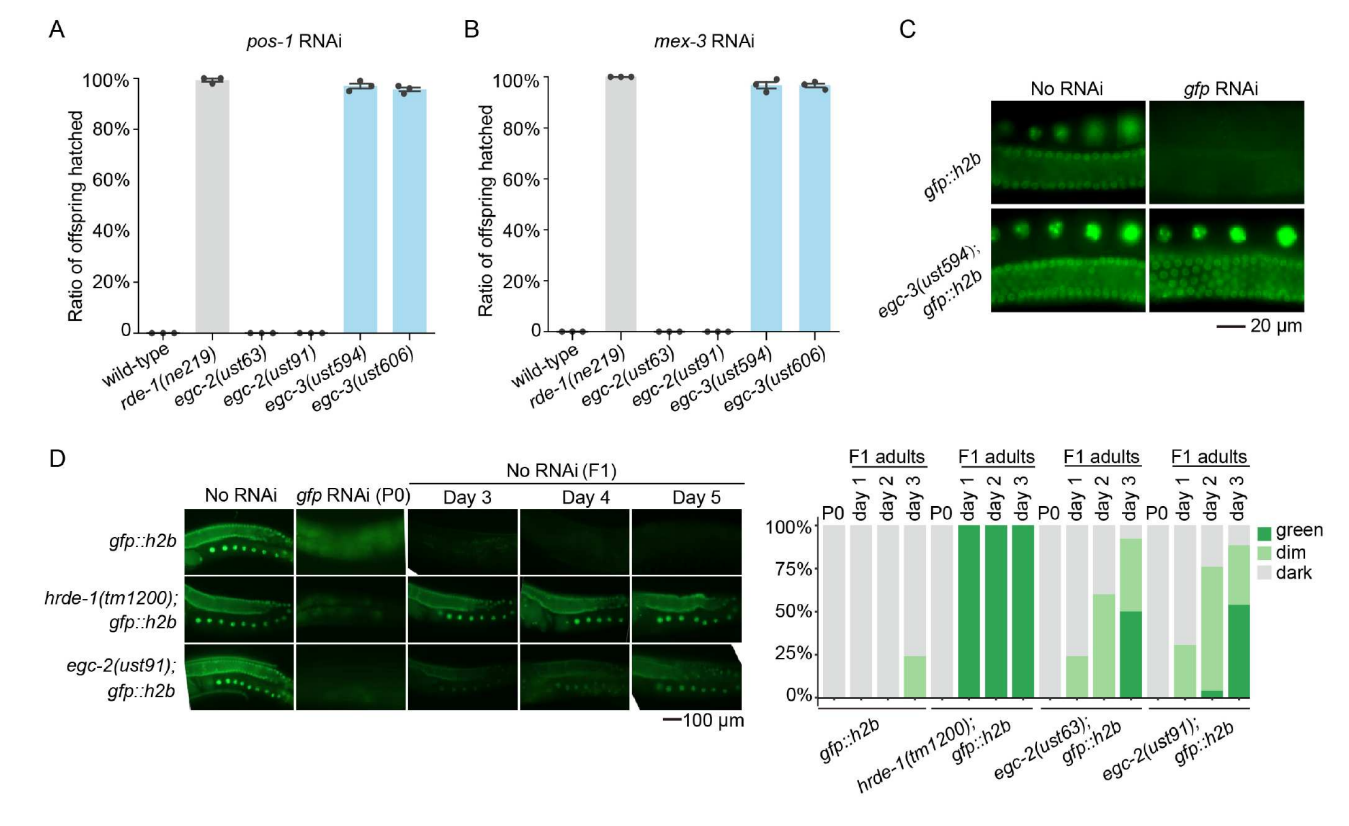


Figure 8. EGC-2 and EGC-3 promote RNA interference. A and B, Bar graphs quantifying the number of hatched embryos following RNAi targeting *pos-1* (A) and *mex-3* (B) in the indicated animals. *mex-3* and *pos-1* encode a KH domain protein and a zinc-finger protein, respectively, both of which are expressed exclusively during embryonic development and are required for early embryonic cell fate decision (Draper et al., 1996; Tabara et al., 1999). Hatched animals were fed bacteria expressing dsRNA targeting *mex-3* or *pos-1* genes from L1 stage to the adult stage. In wild-type animals, RNAi targeting *mex-3* or *pos-1* induces embryonic arrest (dead embryos) in 100% of the embryos produced by PO animals exposed to dsRNA. C, Fluorescence images of the indicated animals subjected to or not subjected to *gfp* RNAi. Animals expressing GFP::HIS-58 were exposed to *gfp* RNAi, and bleached embryos were cultured on RNAi plates seeded with bacteria expressing *gfp* dsRNA. EGC-3 is required for feeding RNAi targeting germline-expressed GFP. D, Animals expressing GFP::HIS-58 were exposed to *gfp* dsRNA, and bleached F1 progeny were grown in the absence of dsRNA. In wild-type animals, RNAi targeting *gfp* results in the silencing of *gfp::his-58* in 100% of gonads of the PO animals exposed to *gfp* dsRNA, and the silencing effect could be effectively inherited across multiple generations, even without continuously feeding dsRNA to the offspring nematodes. GFP expression in PO adult animals on day 1 and F1 adult animals on days 1, 2, and 3 was imaged by fluorescence microscopy with a 40×objective. Adult day 1 was defined as the 24-h period, etc (Scharf et al., 2021). The percentages of the indicated PO and F1 animals expressing GFP were quantified. The data represent the scoring of at least 30 animals in each generation and for each genotype.

RNA transcripts into E granules and stabilize mRNA intermediates to promote the extension of the EGO module along RNA transcripts to generate siRNAs (Figure 9). Further investigations into the sequence characteristics and processing patterns of RNA intermediates in E granules, as well as the proteins binding to these transcripts, and developing new techniques to profile and image RNA molecules within E granules, may help elucidate how these E granule proteins mediate siRNA amplification.

Germ granule compartments and piRNA production

Biomolecular condensates are microscale compartments in eukaryotic cells that lack surrounding membranes, but enclose biomolecules, including proteins and nucleic acids. Yet, whether the positioning of biomolecules in these membraneless organelles is essential for corresponding biological processes is still ambiguous. For example, P body formation is considered a consequence, rather than a driver, of miRNA-mediated gene silencing (Eulalio et al., 2007). In *C. elegans* embryos, MEG-3 recruits to embryonic germ granules a series of translationally repressed ribonucleoprotein complexes that self-associate in the granules, but this recruitment is not systematically selective for

RNA transcripts with germline-specific functions and is not essential for mRNA regulation (Scholl et al., 2024). Similarly, the disruption of the sub-nucleolar organization of the nucleolus upon the loss of NUCL-1, a homolog of Nucleoli in C. elegans, did not elicit severe growth defects or sterility, implying that the specific architecture of the nucleolus may not be essential for the sequential processing of ribosomal RNAs in C. elegans (Spaulding et al., 2022). Furthermore, different protein components of particular molecular condensates may also exert different regulatory effects on the same biological process. For example, although ZNFX-1, WAGO-4, LOTR-1, and MIP-2 localize in Z granules, the first two proteins (ZNFX-1 and WAGO-4) promote the inheritance of RNAi (Ishidate et al., 2018; Wan et al., 2018; Xu et al., 2018), while both lotr-1 and mip-2 mutants display enhanced RNAi inheritance (Marnik et al., 2022; Price et al., 2023), suggesting that Z granules may play multiple roles in RNAi inheritance. In this study, we identified two intrinsically disordered proteins, EGC-2 and EGC-3, that were enriched in E granules and act as upstream regulators of E granule assembly. We systematically investigated the functions of most known E granule proteins on piRNA production and found that different E granule components may exert distinct regulatory functions on

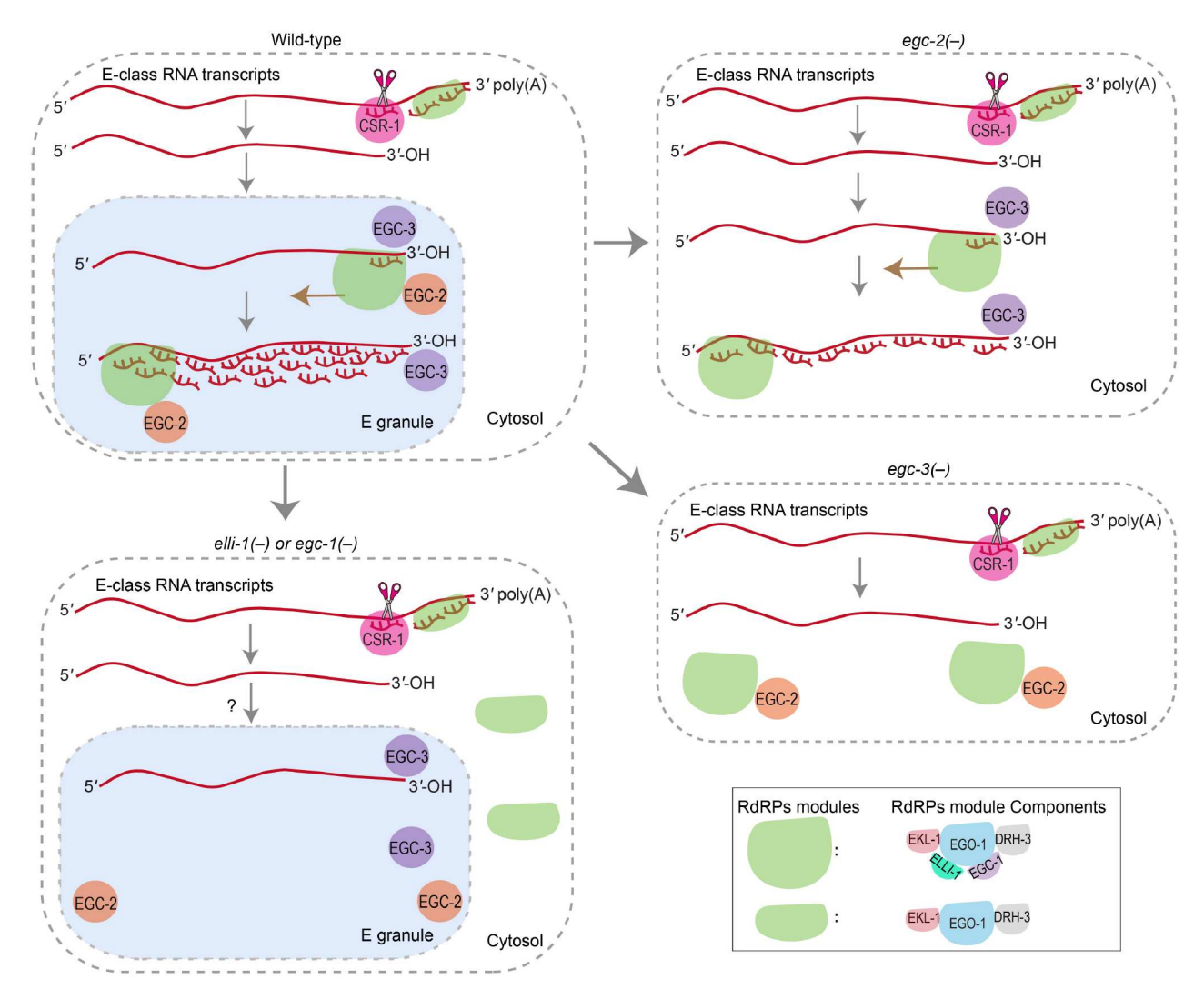


Figure 9. The working model. A model showing the roles of EGC-2 and EGC-3 in E granule assembly and siRNA production. In wild-type animals, 5' E-class siRNAs are produced in E granules. In the *egc-2* animal, the E granule was disrupted, yet the EGO complex could still perform extension in the cytosol along targeted RNA transcripts, although with reduced efficiency. In *elli-1* and *egc-1* mutants, EGO modules (EGO-1/EKL-1/DRH-3) were incapable of performing the extension step of siRNA amplification, yet the initiation step for the biogenesis of siRNAs mapping to the 3' end regions of E-class RNA transcripts might be unaffected in the cytosol. EGC-3 may facilitate the recruitment of E-class RNA transcripts into E granules and stabilize mRNA intermediates to promote the extension of the EGO module along RNA transcripts to generate siRNAs.

piRNA biogenesis. Specifically, the PICS/PETISCO complex promotes piRNA production, whereas EGC-3 and the EGO complex may limit piRNA production. Strikingly, the depletion of EGC-2 destroys E granule formation without affecting piRNA accumulation. Manipulating condensation without disrupting enzymatic activity or RNA binding can disentangle effects due to the disruption of condensates versus the loss of RNP complex activity (Putnam et al., 2023). Our data suggest that although EGC-2 is required for E granule assembly, the E granule assembly defects per se may not diminish piRNA production. Therefore, the enrichment of the PICS complex in E granules is not essential for piRNA processing, at least under normal laboratory cultivation conditions.

Intracellular condensates are highly multicomponent systems that enclose various RNP bodies, undertaking diverse RNA processing events or sequential biological reactions, especially piRNA processing events (Banani et al., 2017). For instance, in the germline cells of the *Drosophila* egg chamber, many proteins

involved in piRNA processing are enriched in a unique perinuclear structure, the nuage, including the following: Vasa, Aub, AGO3, Krimper, Maelstrom, Spindel-E, Tejas, Vreteno, and so on (Pek et al., 2012). These proteins function sequentially to generate primary piRNAs or ping-pong cycle-derived secondary piRNAs (Czech and Hannon, 2016). Interestingly, the proteins involved in the ping-pong cycle exhibit a hierarchical genetic interaction for their localization to the nuage, which could be an indication of their sequential order of function in piRNA biogenesis (Findley et al., 2003; Lim and Kai, 2007; Patil and Kai, 2010). Similarly, in C. elegans germ cells, many piRNA biogenesis factors are enriched in different germ granule compartments, including the E granule-enriched PICS/PETISCO complex, Z granule-enriched PARN-1, and P granule-enriched HENN-1 (Cordeiro Rodrigues et al., 2019; Huang et al., 2025; Kamminga et al., 2012; Tang et al., 2016; Zeng et al., 2019). Additionally, the C. elegans PIWI protein PRG-1 is present in both the Z and P granules, with a preference for the Z granule (Huang

et al., 2025; Wallis and Phillips, 2025). The above pattern of the positioning of piRNA processing factors suggests that piRNA may be sequentially processed across different germ granule compartments in *C. elegans* germ cells. However, our findings in this study suggest that E granule assembly defects generally do not diminish mature piRNA abundance, indicating that disrupting the perinuclear localization of the PICS/PETISCO complex may not affect the subsequent processing of piRNA precursors. Further studies are needed to examine whether and how the perinuclear localization of other piRNA processing factors regulates piRNA production and the piRNA surveillance pathway.

EGC-3 regulates siRNA homeostasis and piRNA production

In the C. elegans germline, the siRNA pathways regulate the expression of thousands of genes, and the homeostasis of siRNAome is closely linked to mRNAome (Billi et al., 2014; Ketting and Cochella, 2021). For example, the aberrant accumulation of siRNAs targeting sid-1 and rde-11 in meg-3/ meg-4 animals leads to abnormal silencing events of their target genes, consequently resulting in defects in the feeding RNAi response (Dodson and Kennedy, 2019; Lev et al., 2019; Ouvang et al., 2019). In this study, we found that the loss of EGC-2 causes mild defects in siRNA amplification, while the depletion of EGC-3 severely disrupts the homeostasis of siRNAome, which may result in distinct phenotypic outcomes of egc-2 and egc-3 mutants. For instance, the aberrant accumulation of siRNAs targeting sid-1 and rde-11 in egc-3 mutants may silence sid-1 and rde-11 genes, respectively, disrupting the feeding RNAi response; yet, siRNAs targeting sid-1 and rde-11 are largely unchanged in egc-2 mutants. Additionally, siRNAs targeting the 5' portion of prg-1 are completely depleted upon the loss of EGC-3, which may increase the production of PRG-1 proteins, ultimately resulting in the overaccumulation of piRNAs, while the siRNAs are only slightly downregulated in the egc-2 mutant. egc-1 and elli-1 mutants show alterations of siRNAomes similar to those of the egc-3 mutant, and exhibit the same phenotypic outcomes, such as the defect in feeding RNAi response and the overaccumulation of piRNAs (Chen et al., 2024). Interestingly, prg-1 mRNA level is dramatically upregulated upon the loss of the EGO complex, yet is largely unaffected in egc-3 animals, hinting that siRNAs mapping to the 5' portion of prg-1 may restrain PRG-1 protein synthesis at the translational level, possibly via directly inhibiting translation processes or indirectly regulating the subcellular localization of prg-1 mRNAs, for example enclosing them in germ granules, which ultimately led to the downregulation of PRG-1 protein levels. Further studies are needed to clarify the functions of 5' Eclass siRNAs in gene expression regulation, especially how the prg-1 siRNAs regulate the level of PRG-1 proteins. Furthermore, deciphering the protein-protein interaction network of EGC-3 may help illustrate the molecular mechanism by which EGC-3 suppresses piRNA production.

MATERIALS AND METHODS

C. elegans strains

The Bristol strain N2 was used as an untagged control in the proximity labeling assay and the standard wild-type strain in RNA-seq analysis. All other strains used in this study were generated by genome editing or genetic crosses and are listed in

Table S2. Unless otherwise indicated, the animals were cultured at 20°C according to standard methods (Brenner, 1974).

Construction of transgenic and mutant strains

For the TurboID transgene, the coding sequence of TurboID fused to a 6AA (amino acid) linker sequence (GGAGGTGGAGGTG-GAGCT) was inserted upstream of the elli-1 stop codon via the CRISPR/Cas9 genome editing method (Cho et al., 2020; Huang et al., 2025). The TurboID sequence was PCR amplified from the plasmid pAS31 (Branon et al., 2018). Left and right homologous arms were PCR amplified from N2 genomic DNA. The vector backbone was PCR amplified from the plasmid pCFJ151. All these fragments were joined together by Gibson assembly to form the repair plasmid using the ClonExpress MultiS One Step Cloning Kit (Vazyme, Nanjing, China). The injection mixture contained the repair plasmid (50 ng μ L⁻¹), pDD162 (50 ng μ L⁻¹), co-injection marker pSG259 (5 ng μL⁻¹) and four sgRNAs targeting 3' elli-1 sequence (30 ng μL⁻¹ of each sgRNA). Three days later, F1 animals expressing pharyngeal GFP were isolated. After another three days, the targeted animals with TurboID insertion were screened via PCR.

For the *drh-3::degron(ust379)* alleles, the injection mixture contained PDD162 (50 ng μL^{-1}), the *drh-3::degron* repair plasmid (50 ng μL^{-1}), pSG258 (5 ng μL^{-1}), and two sgRNAs (30 ng μL^{-1} per sgRNA). The mixture was injected into young adult CA1199 (sun-1p::TIR1::mRuby::sun-1 3'UTR) animals. Targeted animals with *degron* insertions were screened via PCR.

For the *egc-2::gfp::3xflag* ectopic transgene, the DNA elements were fused and integrated into *C. elegans* chromosome II (ttTi5605 locus) via the MosSCI method (Frøkjær-Jensen et al., 2008). For *in situ* tagging of *egc-3*, the coding sequence of *gfp::3xflag* was inserted upstream of the *egc-3* stop codon via the CRISPR/Cas9 method. Plasmids containing repair templates were generated using the ClonExpress MultiS One Step Cloning Kit. The method of obtaining integrated animals through microinjection and PCR screening was the same as above.

For deletion mutants, three or four sgRNAs (30 ng μL^{-1} of each sgRNA) were co-injected into N2 animals with pDD162 (50 ng μL^{-1}), pSG259 (5 ng μL^{-1}). Three days later, F1 animals expressing pharyngeal GFP were isolated. After another three days, the deletion mutants were screened via PCR as previously described (Chen et al., 2014).

Fluorescent streptavidin staining

Synchronized L1 animals were first cultured at 15° C to late L4 stage, and then at 25° C until young adult, since culturing animals at higher temperatures (25° C) increases biotinylation activity (Sanchez et al., 2021; Sanchez and Feldman, 2021). Young adult animals were suspended and washed three times with M9 buffer to remove excess bacteria. The animals were then transferred to CXY buffer ($0.4 \times M9$, $0.1 \text{ mol L}^{-1} \text{ NaN}_3$) and dissected on poly-L-lysine-Prep Slides (Sangon Biotech, Shanghai, China). The dissected animals on the slides were treated with 3.3% (w/v) paraformaldehyde fixation solution in PBS at room temperature for 15 min, followed by two washes with PBS. Slides were then fixed for 15 min in -20° C methanol and washed twice in PBST, after which 1:1,000 streptavidin-Alexa Fluor 488 (Invitrogen, USA) in PBST was added to the slides. The slides were kept in a humidified chamber overnight at 4° C. The slides

were then washed four times with PBST and two times with PBS. Each wash lasted 5 min. Anti-fade Mounting Medium (Sangon Biotech) was added to the slides and covered with a coverslip. The slides were sealed with nail polish and kept at 4° C until imaging.

Streptavidin-HRP blotting

Whole worm lysates were prepared by heating animals in BeyoGel^TM LDS sample buffer (Beyotime, Shanghai, China) at 70°C for 10 min (20 μL of worms, $50~\mu\text{L}$ of $4\times\text{LDS}$ buffer and $130~\mu\text{L}$ of ddH $_2\text{O}$). After centrifugation, $20~\mu\text{L}$ of the supernatant were separated on $4\%{-}12\%$ Bis-Tris gels (Epizyme, USA), and then transferred onto NC membranes, and probed with HRP-conjugated Streptavidin 1:4,000 (Sangon Biotech) for detection via highly sensitive ECL luminescence reagent.

Streptavidin affinity pull-down and mass spectrometry analysis

Approximately 70,000 synchronized L1 animals were placed on NGM plates seeded with concentrated OP50 food and cultured as described previously (Price et al., 2021). Young adults were collected and washed with M9 buffer more than three times to remove excess biotin. Animals were then resuspended in RIPA buffer (50 mmol L^{-1} Tris-HCl (pH 8.0), 150 mmol L^{-1} NaCl, 1% Triton X-100, 0.1% SDS, and 1 mmol L^{-1} EDTA in ddH₂O) supplemented with cOmplete protease inhibitor cocktail (Roche, Switzerland) and solution P. The solution P contained 5 mg/ 10 mL pepstatin A and 0.1 mol L⁻¹ PMSF. The resuspended pellets of the animals were then subjected to liquid nitrogen freezing and grinding cycles until they were ground into powder. The lysates were subsequently centrifuged at $1,6000 \times g$ for 30 min. Zeba Spin Desalting Columns (Thermo Fisher, USA) were used for the desalination and removal of biotin. The supernatant was mixed with Streptavidin magnetic beads (Thermo Fisher) at a ratio of 40 µL beads/500 µL proteins and was incubated overnight at 4°C with constant rotation. Beads were then washed for 5 min, two times with RIPA buffer, once with 1 mol L^{-1} KCl, once with $0.1 \text{ mol } L^{-1} \text{ Na}_2 \text{CO}_3$, and once with 2 mol L^{-1} urea in 10 mmol L^{−1} Tris-HCl (pH 8.0). Beads were subsequently resuspended in PBS and subjected to on-beads trypsin digestion. The bound proteins on the beads were dissolved in $50 \text{ mmol } L^{-1}$ Tris-HCl (pH 8.0) supplemented with 8 mol L-1 urea and 5 mmol L⁻¹ DTT and incubated at 37°C for 1 h with shaking. After incubation, 1 mol L^{−1} iodoacetamide (Sigma, USA) was added to a final concentration of 15 mmol L⁻¹, and the samples were incubated for an additional 30 minutes in the dark at room temperature. The samples were then diluted with three volumes of 50 mmol L⁻¹ Tris-HCl (pH 8.0) to allow for trypsin digestion. 1 ug sequencing grade-modified trypsin (Promega, USA) was mixed with the samples and incubated overnight at 37°C with shaking. The reaction was quenched by adding 2% FA (Sigma) for acidification. The supernatant was taken out and concentrated for LC-MS analysis.

Candidate-based RNAi screening

All RNAi assays were performed at 20°C by placing synchronized embryos on RNAi plates as previously described (Timmons et al., 2001). HT115 bacteria expressing the empty vector L4440 (a gift from A. Fire) were used as controls. Bacterial clones expressing

double-stranded RNAs (dsRNAs) were obtained from the Ahringer RNAi library and sequenced to verify their identity. All feeding RNAi assays were performed for two generations except for sterile animals, which were RNAi-treated for one generation.

RNA isolation and sequencing

Synchronized young adult animals were incubated with TRIzol (Invitrogen) for five quick liquid nitrogen freeze-thaw cycles before isopropanol precipitation. For 21U-RNA sequencing, RNA samples were subjected to DNase I digestion (Thermo Fisher) and re-extracted via the TRIzol method. For 22G-RNA sequencing, samples were further treated with RNA 5'-polyphosphatase (Epicentre) as previously described (Chen et al., 2024).

The prepared RNA samples were subjected to deep sequencing via an Illumina platform (Novogene Bioinformatic Technology Co., Ltd., Beijing, China). Briefly, small RNAs ranging from 17 to 30 nt were gel purified and ligated to a 3' adaptor (5'-pUCGUAUGCCGUCUUCUGCUUGidT-3') and a 5' adaptor (5'-GUUCAGAGUUCUACAGUCCGACGAUC-3'). The ligation products were gel-purified, reverse transcribed, and amplified via Illumina's sRNA primer set (5'-CAAGCAGAAGACGCATACGA-3'; 5'-AATGATACGGCGACCACCGA-3'). The samples were then sequenced via the Illumina HiSeq platform.

RNA-seq analysis

The Illumina-generated raw reads were first filtered to remove adaptors, low-quality tags, and contaminants to obtain clean reads at Novogene. For mature piRNA analysis, clean reads ranging from 17 to 35 nt were respectively mapped to mature piRNA regions, pre-piRNA regions, and the C. elegans transcriptome assembly WS243 using Bowtie2 with default parameters (Zeng et al., 2019). For 22G-RNA analysis, clean reads ranging from 17 to 30 nt, processed by Novogene, were mapped to the C. elegans transcriptome assembly WS243 as previously described (Chen et al., 2024). The number of reads targeting each transcript was counted using custom Perl scripts. The number of total reads mapped to the transcriptome minus the number of total reads corresponding to sense ribosomal RNA (rRNA) transcripts (5S, 5.8S, 18S, and 26S) were used as the normalization number to exclude the possible degradation fragments of sense rRNAs. A cutoff criterion of a twofold change was applied to identify the differentially expressed small RNAs. Scatter plots and Venn diagrams were generated via custom R scripts and modified in Adobe Illustrator. 22G RNA reads were aligned to the C. elegans genome WBcel235 via Bowtie2 v.2.2.5 with default parameters, and IGV v.2.5.3 was used to visualize the alignment results.

Metagene analysis

The metagene profiles were generated according to a method described previously (Singh et al., 2021). The BigWig files were generated using the Snakemake workflow (https://gitlab.Pasteur.fr/bli/bioinfo_utils). Briefly, the 3' adapters and 5' adapters were trimmed from the raw reads using Cutadapt v.1.18 with the following parameters: -a AGATCGGAAGAGCACACGTCT -g GTTCAGAGTTCTACAGTCCGACGATC -discard-untrimmed. After adapter trimming, the reads containing 18 to 26 nt were

selected using Bioawk (https://github.com/lh3/bioawk). The selected 18–26 nucleotide reads were aligned to the *C. elegans* genome (ce11, *C. elegans* Sequencing Consortium WBcel235) using Bowtie2 v.2.3.4.3 with the following parameters: -L 6 -i S,1,0.8 -N 0. The resulting lignments were used to generate bigwig files with a custom bash script using BEDtools version 2.27.1, BEDOPS version 2.4.35, and bedGraphToBigWig version 4. Read counts in the bigwig file were normalized to million "nonstructural" mappers, that is, reads containing 18–26 nt and mapped to annotations not belonging to "structural" (tRNA, snRNA, snoRNA, rRNA, ncRNA) categories and counted using feature Counts77 v.1.6.3. These bigwig files were used to generate "metaprofiles" files with a shell script.

Auxin treatment

Auxin treatment was performed as previously reported (Jin et al., 2025).

Brood size

Synchronized L4 hermaphrodites were singled onto NGM plates and transferred daily as adults until embryo production ceased. The total number of progenies produced was counted.

Microscope and images

To image young adults, the animals were immobilized in ddH_2O with $0.5~mol~L^{-1}~NaN_3$ and mounted on 2% agarose pads. To image germ cells and embryos, the animals were dissected in CXY buffer $(0.4\times M9,~0.1~mol~L^{-1}~NaN_3)$ on a coverslip and then mounted on 1.3%-1.5% agarose pads. Images were collected using a Leica upright DM4 B microscope equipped with a Leica (Germany) DFC7000 T camera. For stitched images, individual images were collected by shifting the slides horizontally and then stitched manually in overlapping regions.

Statistics

The bar graphs with error bars represent the mean \pm SDs. All experiments were performed with independent animal samples or the indicated number of replicates. Statistical analysis was performed with a two-tailed Student's t-test.

Data availability

The raw sequence data reported in this paper have been deposited in the Genome Sequence Archive in the National Genomics Data Center (China National Center for Bioinformation/Beijing Institute of Genomics, Chinese Academy of Sciences) under accession codes CRA019966, CRA019967, and CRA019969.

Compliance and ethics

The authors declare that they have no conflict of interest.

Acknowledgement

This work was supported by the National Key Research and Development Program of China (2022YFA1302700), the National Natural Science Foundation of China (32230016, 32270583, 32470633, 32400435, 2023M733425, 32300438), the Research Funds of Center for Advanced Interdisciplinary Science and Biomedicine of IHM (QYPY20230021), the Fundamental Research Funds for the Central Universities. We are grateful to the members of the Guang laboratory for their comments. We are grateful to Dr. Gang Wan's laboratory for the

suggestions and technical support. We are grateful to the International *C. elegans* Gene Knockout Consortium and the National Bioresource Project for providing the strains. Some strains were provided by the CGC, which is funded by the NIH Office of Research Infrastructure Programs (P40 OD010440)

Supporting information

The supporting information is available online at https://doi.org/10.1007/s11427-025-3025-6. The supporting materials are published as submitted, without typesetting or editing. The responsibility for scientific accuracy and content remains entirely with the authors.

References

- Andralojc, K.M., Campbell, A.C., Kelly, A.L., Terrey, M., Tanner, P.C., Gans, I.M., Senter-Zapata, M.J., Khokhar, E.S., Updike, D.L., and Copenhaver, G.P. (2017). ELLI-1, a novel germline protein, modulates RNAi activity and P-granule accumulation in Caenorhabditis elegans. PLoS Genet 13, e1006611.
- Aoki, S.T., Lynch, T.R., Crittenden, S.L., Bingman, C.A., Wickens, M., and Kimble, J. (2021). C. elegans germ granules require both assembly and localized regulators for mRNA repression. Nat Commun 12, 996.
- Ashe, A., Sapetschnig, A., Weick, E.M., Mitchell, J., Bagijn, M.P., Cording, A.C., Doebley, A.L., Goldstein, L.D., Lehrbach, N.J., Le Pen, J., et al. (2012). piRNAs can rigger a multigenerational epigenetic memory in the germline of *C. elegans*. Cell 150, 88–99.
- Bagijn, M.P., Goldstein, L.D., Sapetschnig, A., Weick, E.M., Bouasker, S., Lehrbach, N. J., Simard, M.J., and Miska, E.A. (2012). Function, targets, and evolution of *Caenorhabditis elegans* piRNAs. Science 337, 574–578.
- Banani, S.F., Lee, H.O., Hyman, A.A., and Rosen, M.K. (2017). Biomolecular condensates: organizers of cellular biochemistry. Nat Rev Mol Cell Biol 18, 285– 298
- Batista, P.J., Ruby, J.G., Claycomb, J.M., Chiang, R., Fahlgren, N., Kasschau, K.D., Chaves, D.A., Gu, W., Vasale, J.J., Duan, S., et al. (2008). PRG-1 and 21U-RNAs interact to form the piRNA complex required for fertility in *C. elegans*. Mol Cell 31, 67–78.
- Billi, A.C., Fischer, S.E.J., and Kim, J.K. (2014). Endogenous RNAi pathways in *C. elegans*. WormBook doi: 10.1895/wormbook.1.170.1.
- Boeynaems, S., Alberti, S., Fawzi, N.L., Mittag, T., Polymenidou, M., Rousseau, F., Schymkowitz, J., Shorter, J., Wolozin, B., Van Den Bosch, L., et al. (2018). Protein phase separation: a new phase in cell biology. Trends Cell Biol 28, 420–435.
- Brangwynne, C.P., Eckmann, C.R., Courson, D.S., Rybarska, A., Hoege, C., Gharakhani, J., Jülicher, F., and Hyman, A.A. (2009). Germline P granules are liquid droplets that localize by controlled dissolution/condensation. Science 324, 1729–1732.
- Branon, T.C., Bosch, J.A., Sanchez, A.D., Udeshi, N.D., Svinkina, T., Carr, S.A., Feldman, J.L., Perrimon, N., and Ting, A.Y. (2018). Efficient proximity labeling in living cells and organisms with TurboID. Nat Biotechnol 36, 880–887.
- Brenner, S. (1974). The genetics of Caenorhabditis elegans. Genetics 77, 71-94.
- Chen, S., and Phillips, C.M. (2024). HRDE-2 drives small RNA specificity for the nuclear Argonaute protein HRDE-1. Nat Commun 15, 957.
- Chen, S., and Phillips, C.M. (2025). Nuclear Argonaute protein NRDE-3 switches small RNA partners during embryogenesis to mediate temporal-specific gene regulatory activity. eLife 13, RP102226.
- Chen, W., Hu, Y., Lang, C.F., Brown, J.S., Schwabach, S., Song, X., Zhang, Y., Munro, E., Bennett, K., Zhang, D., et al. (2020). The dynamics of P granule liquid droplets are regulated by the *Caenorhabditis elegans* germline RNA helicase GLH-1 via its ATP hydrolysis cycle. Genetics 215, 421–434.
- Chen, W., Brown, J.S., He, T., Wu, W.S., Tu, S., Weng, Z., Zhang, D., and Lee, H.C. (2022). GLH/VASA helicases promote germ granule formation to ensure the fidelity of piRNA-mediated transcriptome surveillance. Nat Commun 13, 5306.
- Chen, X., Wang, K., Mufti, F.U.D., Xu, D., Zhu, C., Huang, X., Zeng, C., Jin, Q., Huang, X., Yan, Y., et al. (2024). Germ granule compartments coordinate specialized small RNA production. Nat Commun 15, 5799.
- Chen, X., Xu, F., Zhu, C., Ji, J., Zhou, X., Feng, X., and Guang, S. (2014). Dual sgRNA-directed gene knockout using CRISPR/Cas9 technology in *Caenorhabditis elegans*. Sci Rep 4, 7581.
- Cho, K.F., Branon, T.C., Udeshi, N.D., Myers, S.A., Carr, S.A., and Ting, A.Y. (2020). Proximity labeling in mammalian cells with TurboID and split-TurboID. Nat Protoc 15, 3971–3999.
- Cipriani, P.G., Bay, O., Zinno, J., Gutwein, M., Gan, H.H., Mayya, V.K., Chung, G., Chen, J.X., Fahs, H., Guan, Y., et al. (2021). Novel LOTUS-domain proteins are organizational hubs that recruit *C. elegans* Vasa to germ granules. eLife 10, e60833.
- Cordeiro Rodrigues, R.J., de Jesus Domingues, A.M., Hellmann, S., Dietz, S., de Albuquerque, B.F.M., Renz, C., Ulrich, H.D., Sarkies, P., Butter, F., and Ketting, R.F. (2019). PETISCO is a novel protein complex required for 21U RNA biogenesis and embryonic viability. Genes Dev 33, 857–870.

- Czech, B., and Hannon, G.J. (2016). One loop to rule them all: the ping-pong cycle and piRNA-guided silencing. Trends Biochem Sci 41, 324–337.
- Dai, S.Y., Tang, X.Y., Li, L.L., Ishidate, T., Ozturk, A.R., Chen, H., Dube, A.L., Yan, Y. H., Dong, M.Q., Shen, E.Z., et al. (2022). A family of *C. elegans* Vasa homologs control Argonaute pathway specificity and promote transgenerational silencing. Cell Rep 40, 111265.
- Das, P.P., Bagijn, M.P., Goldstein, L.D., Woolford, J.R., Lehrbach, N.J., Sapetschnig, A., Buhecha, H.R., Gilchrist, M.J., Howe, K.L., Stark, R., et al. (2008). Piwi and piRNAs act upstream of an endogenous siRNA pathway to suppress Tc3 transposon mobility in the *Caenorhabditis elegans* germline. Mol Cell 31, 79–90.
- Dodson, A.E., and Kennedy, S. (2019). Germ granules coordinate RNA-based epigenetic inheritance pathways. Dev Cell 50, 704–715.e4.
- Dodson, A.E., and Kennedy, S. (2020). Phase separation in germ cells and development. Dev Cell 55, 4–17.
- Draper, B.W., Mello, C.C., Bowerman, B., Hardin, J., and Priess, J.R. (1996). MEX-3 is a KH domain protein that regulates blastomere identity in early C. elegans embryos. Cell 87, 205–216.
- Du, Z., Shi, K., Brown, J.S., He, T., Wu, W.S., Zhang, Y., Lee, H.C., and Zhang, D. (2023). Condensate cooperativity underlies transgenerational gene silencing. Cell Rep 42, 112859.
- Eddy, E.M. (1974). Fine structural observations on the form and distribution of nuage in germ cells of the rat. Anat Rec 178, 731–757.
- Eddy, E.M. (1975). Germ plasm and the differentiation of the germ cell line. Int Rev Cytol 43, 229–280.
- Erdős, G., and Dosztányi, Z. (2024). AIUPred: combining energy estimation with deep learning for the enhanced prediction of protein disorder. Nucleic Acids Res 52, W176–W181.
- Eulalio, A., Behm-Ansmant, I., Schweizer, D., and Izaurralde, E. (2007). P-body formation is a consequence, not the cause, of RNA-Mediated gene silencing. Mol Cell Biol 27, 3970–3981.
- Fare, C.M., Villani, A., Drake, L.E., and Shorter, J. (2021). Higher-order organization of biomolecular condensates. Open Biol 11, 210137.
- Findley, S.D., Tamanaha, M., Clegg, N.J., and Ruohola-Baker, H. (2003). Maelstrom a Drosophila spindle-class gene, encodes a protein that colocalizes with Vasa and RDE1/AGO1 homolog, Aubergine, in nuage. Development 130, 859–871.
- Folkmann, A.W., Putnam, A., Lee, C.F., and Seydoux, G. (2021). Regulation of biomolecular condensates by interfacial protein clusters. Science 373, 1218–1224.
- Frøkjær-Jensen, C., Wayne Davis, M., Hopkins, C.E., Newman, B.J., Thummel, J.M., Olesen, S.P., Grunnet, M., and Jorgensen, E.M. (2008). Single-copy insertion of transgenes in *Caenorhabditis elegans*. Nat Genet 40, 1375–1383.
- Gajjar, G., Huggins, H.P., Kim, E.S., Huang, W., Bonnet, F.X., Updike, D.L., Keiper, B. D., and Kennedy, S. (2025). Two eIF4E paralogs occupy separate germ granule messenger ribonucleoproteins that mediate mRNA repression and translational activation. Genetics 230, iyaf053.
- Goh, W.S.S., Seah, J.W.E., Harrison, E.J., Chen, C., Hammell, C.M., and Hannon, G.J. (2014). A genome-wide RNAi screen identifies factors required for distinct stages of C. elegans piRNA biogenesis. Genes Dev 28, 797–807.
- Goudeau, J., Sharp, C.S., Paw, J., Savy, L., Leonetti, M.D., York, A.G., Updike, D.L., Kenyon, C., Ingaramo, M., and Buelow, H. (2021). Split-wrmScarlet and splitsfGFP: tools for faster, easier fluorescent labeling of endogenous proteins in *Caenorhabditis elegans*. Genetics 217, iyab014.
- Gu, W., Shirayama, M., Conte Jr., D., Vasale, J., Batista, P.J., Claycomb, J.M., Moresco, J.J., Youngman, E.M., Keys, J., Stoltz, M.J., et al. (2009). Distinct argonaute-mediated 22G-RNA pathways direct genome surveillance in the C. elegans germline. Mol Cell 36, 231–244.
- Guillén-Boixet, J., Kopach, A., Holehouse, A.S., Wittmann, S., Jahnel, M., Schlüßler, R., Kim, K., Trussina, I.R.E.A., Wang, J., Mateju, D., et al. (2020). RNA-induced conformational switching and clustering of G3BP drive stress granule assembly by condensation. Cell 181, 346–361.e17.
- Hanazawa, M., Yonetani, M., and Sugimoto, A. (2011). PGL proteins self associate and bind RNPs to mediate germ granule assembly in *C. elegans*. J Cell Biol 192, 929–937.
- Harris, T.W., Arnaboldi, V., Cain, S., Chan, J., Chen, W.J., Cho, J., Davis, P., Gao, S., Grove, C.A., Kishore, R., et al. (2020). WormBase: a modern model organism information resource. Nucleic Acids Res doi: 10.1093/nar/gkz920.
- Hofmann, S., Kedersha, N., Anderson, P., and Ivanov, P. (2021). Molecular mechanisms of stress granule assembly and disassembly. Biochim Biophys Acta 1868, 118876.
- Huang, X., Cheng, P., Weng, C., Xu, Z., Zeng, C., Xu, Z., Chen, X., Zhu, C., Guang, S., and Feng, X. (2021). A chromodomain protein mediates heterochromatin-directed piRNA expression. Proc Natl Acad Sci USA 118, e2103723118.
- Huang, X., Feng, X., Yan, Y.H., Xu, D., Wang, K., Zhu, C., Dong, M.Q., Huang, X., Guang, S., and Chen, X. (2025). Compartmentalized localization of perinuclear proteins within germ granules in C. elegans. Dev Cell 60, 1251–1270.e3.

- Ishidate, T., Ozturk, A.R., Durning, D.J., Sharma, R., Shen, E., Chen, H., Seth, M., Shirayama, M., and Mello, C.C. (2018). ZNFX-1 functions within perinuclear nuage to balance epigenetic signals. Mol Cell 70, 639–649.e6.
- Jin, Q.L., Feng, X., Hong, M., Wang, K., Chen, X., Cheng, J., Kuang, Y., Si, X., Xu, M., Huang, X., et al. (2025). Peri-centrosomal localization of small interfering RNAs in C.elegans. Sci China Life Sci 68, 895–911.
- Kamminga, L.M., van Wolfswinkel, J.C., Luteijn, M.J., Kaaij, L.J.T., Bagijn, M.P., Sapetschnig, A., Miska, E.A., Berezikov, E., Ketting, R.F., and Kim, S.K. (2012). Differential impact of the HEN1 homolog HENN-1 on 21U and 26G RNAs in the germline of *Caenorhabditis elegans*. PLoS Genet 8, e1002702.
- Kawasaki, I., Shim, Y.H., Kirchner, J., Kaminker, J., Wood, W.B., and Strome, S. (1998). PGL-1, a predicted RNA-binding component of germ granules, is essential for fertility in *C. elegans*. Cell 94, 635–645.
- Kemph, A., and Lynch, J.A. (2022). Evolution of germ plasm assembly and function among the insects. Curr Opin Insect Sci 50, 100883.
- Ketting, R.F., and Cochella, L. (2021). Concepts and functions of small RNA pathways in C. elegans. Curr Top Dev Biol 144, 45–89.
- Lafontaine, D.L.J., Riback, J.A., Bascetin, R., and Brangwynne, C.P. (2021). The nucleolus as a multiphase liquid condensate. Nat Rev Mol Cell Biol 22, 165–182.
- Lee, H.C., Gu, W., Shirayama, M., Youngman, E., Conte Jr, D., and Mello, C.C. (2012).
 C. elegans piRNAs mediate the genome-wide surveillance of germline transcripts.
 Cell 150, 78–87.
- Lehmann, R. (2016). Germ plasm biogenesis—an oskar-centric perspective. Curr Top Dev Biol 116, 679–707.
- Lev, I., Toker, I.A., Mor, Y., Nitzan, A., Weintraub, G., Antonova, O., Bhonkar, O., Ben Shushan, I., Seroussi, U., Claycomb, J.M., et al. (2019). Germ granules govern small RNA inheritance. Curr Biol 29, 2880–2891.e4.
- Lim, A.K., and Kai, T. (2007). Unique germ-line organelle, nuage, functions to repress selfish genetic elements in *Drosophila melanogaster*. Proc Natl Acad Sci USA 104, 6714–6719.
- Liu, L., Wang, X., Zhao, W., Li, Q., Li, J., Chen, H., and Shan, G. (2023). Systematic characterization of small RNAs associated with C. elegans Argonautes. Sci China Life Sci 66, 1303–1322.
- Lu, P., Deng, B.Y., Li, X.R., Niu, X.F., Qiu, Y.H., Liang, Y.T., Liang, Y.L., Tang, G.R., Yuan, Z.P., Luo, G.Z., et al. (2025). A nuclear pore-anchored condensate enables germ granule organization and transgenerational epigenetic inheritance. Nat Struct Mol Biol 32, 1241–1254.
- Luteijn, M.J., van Bergeijk, P., Kaaij, L.J.T., Almeida, M.V., Roovers, E.F., Berezikov, E., and Ketting, R.F. (2012). Extremely stable Piwi-induced gene silencing in *Caenorhabditis elegans*. EMBO J 31, 3422–3430.
- Manage, K.I., Rogers, A.K., Wallis, D.C., Uebel, C.J., Anderson, D.C., Nguyen, D.A.H., Arca, K., Brown, K.C., Cordeiro Rodrigues, R.J., de Albuquerque, B.F., et al. (2020). A tudor domain protein, SIMR-1, promotes siRNA production at piRNA-targeted mRNAs in C. elegans. eLife 9, e56731.
- Maniar, J.M., and Fire, A.Z. (2011). EGO-1, a C. elegans RdRP, modulates gene expression via production of mRNA-templated short antisense RNAs. Curr Biol 21, 449–459.
- Marnik, E.A., Almeida, M.V., Cipriani, P.G., Chung, G., Caspani, E., Karaulanov, E., Gan, H.H., Zinno, J., Isolehto, I.J., Kielisch, F., et al. (2022). The *Caenorhabditis elegans* TDRD5/7-like protein, LOTR-1, interacts with the helicase ZNFX-1 to balance epigenetic signals in the germline. PLoS Genet 18, e1010245.
- Mukherjee, N., and Mukherjee, C. (2021). Germ cell ribonucleoprotein granules in different clades of life: from insects to mammals. Wiley Interdiscip Rev RNA 12, e1642.
- Ouyang, J.P.T., Folkmann, A., Bernard, L., Lee, C.Y., Seroussi, U., Charlesworth, A.G., Claycomb, J.M., and Seydoux, G. (2019). P granules protect RNA interference genes from silencing by piRNAs. Dev Cell 50, 716–728.e6.
- Ouyang, J.P.T., Zhang, W.L., and Seydoux, G. (2022). The conserved helicase ZNFX-1 memorializes silenced RNAs in perinuclear condensates. Nat Cell Biol 24, 1129–1140.
- Patil, V.S., and Kai, T. (2010). Repression of retroelements in drosophila germline via piRNA pathway by the tudor domain protein tejas. Curr Biol 20, 724–730.
- Pek, J.W., Patil, V.S., and Kai, T. (2012). piRNA pathway and the potential processing site, the nuage, in the *Drosophila* germline. Dev Growth Differ 54, 66–77.
- Phillips, C.M., Montgomery, T.A., Breen, P.C., and Ruvkun, G. (2012). MUT-16 promotes formation of perinuclear *Mutator* foci required for RNA silencing in the *C. elegans* germline. Genes Dev 26, 1433–1444.
- Phillips, C.M., Updike, D.L., and Kim, J. (2022). Germ granules and gene regulation in the *Caenorhabditis elegans* germline. Genetics 220, iyab195.
- Placentino, M., de Jesus Domingues, A.M., Schreier, J., Dietz, S., Hellmann, S., de Albuquerque, B.F., Butter, F., and Ketting, R.F. (2021). Intrinsically disordered protein PID-2 modulates Z granules and is required for heritable piRNA-induced silencing in the Caenorhabditis elegans embryo. EMBO J 40, e105280.
- Podvalnaya, N., Bronkhorst, A.W., Lichtenberger, R., Hellmann, S., Nischwitz, E.,

- Falk, T., Karaulanov, E., Butter, F., Falk, S., and Ketting, R.F. (2023). piRNA processing by a trimeric Schlafen-domain nuclease. Nature 622, 402–409.
- Price, I.F., Hertz, H.L., Pastore, B., Wagner, J., and Tang, W. (2021). Proximity labeling identifies LOTUS domain proteins that promote the formation of perinuclear germ granules in *C. elegans*. eLife 10, e72276.
- Price, I.F., Wagner, J.A., Pastore, B., Hertz, H.L., and Tang, W. (2023). C. elegans germ granules sculpt both germline and somatic RNAome. Nat Commun 14, 5965.
- Putnam, A., Thomas, L., and Seydoux, G. (2023). RNA granules: functional compartments or incidental condensates? Genes Dev 37, 354–376.
- Ruan, K., Bai, G., Fang, Y., Li, D., Li, T., Liu, X., Lu, B., Lu, Q., Songyang, Z., Sun, S., et al. (2024). Biomolecular condensates and disease pathogenesis. Sci China Life Sci 67, 1792–1832.
- Sanchez, A.D., Branon, T.C., Cote, L.E., Papagiannakis, A., Liang, X., Pickett, M.A., Shen, K., Jacobs-Wagner, C., Ting, A.Y., and Feldman, J.L. (2021). Proximity labeling reveals non-centrosomal microtubule-organizing center components required for microtubule growth and localization. Curr Biol 31, 3586–3600.e11.
- Sanchez, A.D., and Feldman, J.L. (2021). A proximity labeling protocol to probe proximity interactions in C. elegans. STAR Protocols 2, 100986.
- Sanders, D.W., Kedersha, N., Lee, D.S.W., Strom, A.R., Drake, V., Riback, J.A., Bracha, D., Eeftens, J.M., Iwanicki, A., Wang, A., et al. (2020). Competing protein-RNA interaction networks control multiphase intracellular organization. Cell 181, 306–324.e28.
- Scharf, A., Pohl, F., Egan, B.M., Kocsisova, Z., and Kornfeld, K. (2021). Reproductive aging in *Caenorhabditis elegans*: from molecules to ecology. Front Cell Dev Biol 9, 718522
- Scholl, A., Liu, Y., and Seydoux, G. (2024). Caenorhabditis elegans germ granules accumulate hundreds of low translation mRNAs with no systematic preference for germ cell fate regulators. Development 151, dev202575.
- Seroussi, U., Lugowski, A., Wadi, L., Lao, R.X., Willis, A.R., Zhao, W., Sundby, A.E., Charlesworth, A.G., Reinke, A.W., and Claycomb, J.M. (2023). A comprehensive survey of *C. elegans* Argonaute proteins reveals organism-wide gene regulatory networks and functions. eLife 12, e83853.
- Sheth, U., Pitt, J., Dennis, S., and Priess, J.R. (2010). Perinuclear P granules are the principal sites of mRNA export in adult *C. elegans* germ cells. Development 137, 1305–1314.
- Shi, K., Zhang, Y., Du, Z., Liu, S.C., Leon, I., Fan, X., Lee, H.C., and Zhang, D. (2025). Nucleoporins shape germ granule architecture and balance small RNA silencing pathways. Nat Commun 16, 4295.
- Shin, Y., and Brangwynne, C.P. (2017). Liquid phase condensation in cell physiology and disease. Science 357, eagl4382.
- Shirayama, M., Seth, M., Lee, H.C., Gu, W., Ishidate, T., Conte Jr., D., and Mello, C.C. (2012). piRNAs initiate an epigenetic memory of nonself RNA in the *C. elegans* germline. Cell 150, 65–77.
- Singh, M., Cornes, E., Li, B., Quarato, P., Bourdon, L., Dingli, F., Loew, D., Proccacia, S., and Cecere, G. (2021). Translation and codon usage regulate Argonaute slicer activity to trigger small RNA biogenesis. Nat Commun 12, 3492.
- Spaulding, E.L., Feidler, A.M., Cook, L.A., and Updike, D.L. (2022). RG/RGG repeats in the *C. elegans* homologs of Nucleolin and GAR1 contribute to sub-nucleolar phase separation. Nat Commun 13, 6585.
- Standart, N., and Weil, D. (2018). P-bodies: cytosolic droplets for coordinated mRNA storage. Trends Genet 34, 612–626.
- Sundby, A.E., Molnar, R.I., and Claycomb, J.M. (2021). Connecting the dots: linking Caenorhabditis elegans small RNA pathways and germ granules. Trends Cell Biol 31, 387–401.
- Tabara, H., Hill, R.J., Mello, C.C., Priess, J.R., and Kohara, Y. (1999). pos-1 encodes a cytoplasmic zinc-finger protein essential for germline specification in C. elegans. Development 126, 1–11.
- Tang, W., Tu, S., Lee, H.C., Weng, Z., and Mello, C.C. (2016). The RNase PARN-1 trims piRNA 3' ends to promote transcriptome surveillance in C. elegans. Cell 164, 974–984
- Thomas, L.L., Bodas, D.M., and Seydoux, G. (2025). FG repeats drive co-clustering of nuclear pores and P granules in the C. elegans germline. Development 152, dev204585.
- Timmons, L., Court, D.L., and Fire, A. (2001). Ingestion of bacterially expressed dsRNAs can produce specific and potent genetic interference in *Caenorhabditis elegans*. Gene 263, 103–112.
- Toretsky, J.A., and Wright, P.E. (2014). Assemblages: functional units formed by cellular phase separation. J Cell Biol 206, 579–588.

- Uebel, C.J., Anderson, D.C., Mandarino, L.M., Manage, K.I., Aynaszyan, S., Phillips, C. M., and Miska, E.A. (2018). Distinct regions of the intrinsically disordered protein MUT-16 mediate assembly of a small RNA amplification complex and promote phase separation of *Mutator* foci. PLoS Genet 14, e1007542.
- Uebel, C.J., Rajeev, S., and Phillips, C.M. (2023). Caenorhabditis elegans germ granules are present in distinct configurations and assemble in a hierarchical manner. Development 150, dev202284.
- Updike, D., and Strome, S. (2010). P granule assembly and function in *Caenorhabditis elegans* germ cells. J Andrology 31, 53–60.
- Updike, D.L., and Strome, S. (2009). A genomewide RNAi screen for genes that affect the stability, distribution and function of P granules in *Caenorhabditis elegans*. Genetics 183, 1397–1419.
- Voronina, E., and Seydoux, G. (2010). The C. elegans homolog of nucleoporin Nup98 is required for the integrity and function of germline P granules. Development 137, 1441–1450
- Voronina, E., Seydoux, G., Sassone-Corsi, P., and Nagamori, I. (2011). RNA granules in germ cells. Cold Spring Harb Perspect Biol 3, a002774.
- Wallis, D.C., and Phillips, C.M. (2025). RG motifs promote piRNA-mediated gene silencing in C. elegans. bioRxiv, 2025, 653514.
- Wan, G., Bajaj, L., Fields, B., Dodson, A.E., Pagano, D., Fei, Y., and Kennedy, S. (2021). ZSP-1 is a Z granule surface protein required for Z granule fluidity and germline immortality in *Caenorhabditis elegans*. EMBO J 40, e105612.
- Wan, G., Fields, B.D., Spracklin, G., Shukla, A., Phillips, C.M., and Kennedy, S. (2018). Spatiotemporal regulation of liquid-like condensates in epigenetic inheritance. Nature 557, 679–683.
- Wang, G., and Reinke, V. (2008). A C. elegans Piwi, PRG-1, regulates 21U-RNAs during spermatogenesis. Curr Biol 18, 861–867.
- Wang, J.T., Smith, J., Chen, B.C., Schmidt, H., Rasoloson, D., Paix, A., Lambrus, B.G., Calidas, D., Betzig, E., and Seydoux, G. (2014). Regulation of RNA granule dynamics by phosphorylation of serine-rich, intrinsically disordered proteins in *C. elegans*, eLife 3, e04591.
- Wang, Y.H., Hertz, H.L., Pastore, B., and Tang, W. (2025). An AT-hook transcription factor promotes transcription of histone, spliced-leader, and piRNA clusters. Nucleic Acids Res 53. gkaf079.
- Winston, W.M., Molodowitch, C., and Hunter, C.P. (2002). Systemic RNAi in C. elegans requires the putative transmembrane protein SID-1. Science 295, 2456– 2459.
- Xu, F., Feng, X., Chen, X., Weng, C., Yan, Q., Xu, T., Hong, M., and Guang, S. (2018).
 A cytoplasmic Argonaute protein promotes the inheritance of RNAi. Cell Rep 23, 2482–2494.
- Yanagawa, M., and Shimobayashi, S.F. (2024). Multi-dimensional condensation of intracellular biomolecules. J Biochem 175, 179–186.
- Yang, H., Zhang, Y., Vallandingham, J., Li, H., Florens, L., and Mak, H.Y. (2012). The RDE-10/RDE-11 complex triggers RNAi-induced mRNA degradation by association with target mRNA in *C. elegans*. Genes Dev 26, 846–856.
- Yang, P., Mathieu, C., Kolaitis, R.M., Zhang, P., Messing, J., Yurtsever, U., Yang, Z., Wu, J., Li, Y., Pan, Q., et al. (2020). G3BP1 is a tunable switch that triggers phase separation to assemble stress granules. Cell 181, 325–345.e28.
- Zeng, C., Weng, C., Wang, X., Yan, Y.H., Li, W.J., Xu, D., Hong, M., Liao, S., Dong, M. Q., Feng, X., et al. (2019). Functional proteomics identifies a PICS complex required for piRNA maturation and chromosome segregation. Cell Rep 27, 3561–3572.e3.
- Zhang, C., Montgomery, T.A., Fischer, S.E.J., Garcia, S.M.D.A., Riedel, C.G., Fahlgren, N., Sullivan, C.M., Carrington, J.C., and Ruvkun, G. (2012). The *Caenorhabditis elegans* RDE-10/RDE-11 complex regulates RNAi by promoting secondary siRNA amplification. Curr Biol 22, 881–890.
- Zhang, C., Montgomery, T.A., Gabel, H.W., Fischer, S.E.J., Phillips, C.M., Fahlgren, N., Sullivan, C.M., Carrington, J.C., and Ruvkun, G. (2011). mut-16 and other Mutator class genes modulate 22G and 26G siRNA pathways in Caenorhabditis elegans. Proc Natl Acad Sci USA 108, 1201–1208.
- Zhang, L., Ward, J.D., Cheng, Z., and Dernburg, A.F. (2015). The auxin-inducible degradation (AID) system enables versatile conditional protein depletion in C. elegans. Development 142, 4374–4384.
- Zhang, W.J, and Wang, Y. (2023). Activating translation by phase separation: a novel mechanism for driving spermiogenesis. Sci China Life Sci 66, 418–420.
- Zhao, C., Cai, S., Shi, R., Li, X., Deng, B., Li, R., Yang, S., Huang, J., Liang, Y., Lu, P., et al. (2024). HERD-1 mediates multiphase condensate immiscibility to regulate small RNA-driven transgenerational epigenetic inheritance. Nat Cell Biol 26, 1958–1970